

Acoustic Holography

26. Acoustic Holography

Yang-Hann Kim

One of the subtle problems that make noise control difficult for engineers is the invisibility of noise or sound. A visual image of noise often helps to determine an appropriate means for noise control. There have been many attempts to fulfill this rather challenging objective. Theoretical (or numerical) means for visualizing the sound field have been attempted, and as a result, a great deal of progress has been made. However, most of these numerical methods are not quite ready for practical applications to noise control problems. In the meantime, rapid progress with instrumentation has made it possible to use multiple microphones and fast signal-processing systems. Although these systems are not perfect, they are useful. A state-of-the-art system has recently become available, but it still has many problematic issues; for example, how can one implement the visualized noise field. The constructed noise or sound picture always consists of bias and random errors, and consequently, it is often difficult to determine the origin of the noise and the spatial distribution of the noise field. Section 26.2 of this chapter introduces a brief history, which is associated with *sound visualization*, acoustic source identification methods and what has been accomplished with a line or surface array. Section 26.2.3 introduces difficulties and recent studies, including de-Dopplerization and de-re-

26.1	The Methodology of Acoustic Source Identification	1115
26.2	Acoustic Holography: Measurement, Prediction and Analysis	1117
26.2.1	Introduction and Problem Definitions	1117
26.2.2	Prediction Process	1118
26.2.3	Measurement	1123
26.2.4	Analysis of Acoustic Holography ..	1127
26.3	Summary	1130
26.A	Mathematical Derivations of Three Acoustic Holography Methods and Their Discrete Forms	1130
26.A.1	Planar Acoustic Holography	1130
26.A.2	Cylindrical Acoustic Holography...	1132
26.A.3	Spherical Acoustic Holography	1133
	References	1133

verberation methods, both essential for visualizing a moving noise source, such as occurs for cars or trains. This section also addresses what produces ambiguity in realizing real sound sources in a room or closed space. Another major issue associated with sound/noise visualization is whether or not we can distinguish between mutual dependencies of noise in space (Sect. 26.2.4); for example, we are asked to answer the question, *Can we see two birds singing or one bird with two beaks?*

26.1 The Methodology of Acoustic Source Identification

The famous article written by *Kac* [26.1], *Can one hear the shape of the drum?* clearly addresses the essence of the inverse problem. It can be regarded as an attempt to obtain what is *not* available, using what is available, using the example of the relationship between sound generation by membrane vibration and its reception in space. One can find many other examples of inverse problems [26.2–8]. Often, in the inverse prob-

lem, it is hard to predict or describe data that are not measured because the available data are insufficient. This circumstance is commonly referred to as an *ill-posed problem* in the literature [26.1–19]. Figure 26.1 demonstrates what might happen in practice; the prediction depends on how well the basis function (the elephants or dogs in Fig. 26.1) mimics what happens in reality. When we try to see the shape of noise/sound

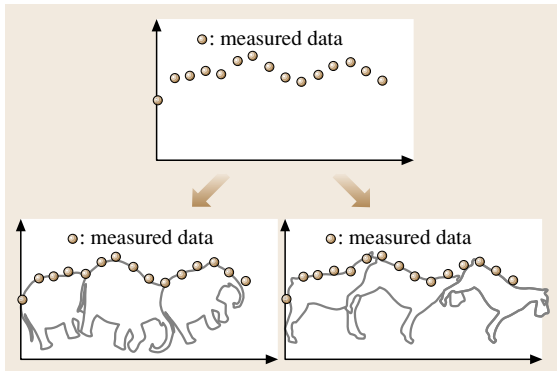


Fig. 26.1 The inverse problem and basis function. Are the measured data the parts of elephants or dogs?

sources, how well we see the shape of a noise source completely depends on this basis function, because we predict what is not available by using this selected basis function.

One of the common methods of classifying methods used in noise/sound source identification, is by the type of basis function. According to this classification, one approach is the nonparametric method, which uses basis functions that do not model the signal. In other words, the basis functions do not map the unmeasured sound field; all orthogonal functions fall into this category. One of the typical methods of this kind uses Fourier transforms. Acoustic holography uses this type of basis function, mapping the sound field of interest

with regard to every measured frequency; it therefore sees the sound field in the frequency domain. In fact, the ideas of acoustic holography originated from optics [26.20–30]. Acoustic holography was simply extended or modified from the basic idea of optical holography. Near-field acoustic holography [26.31,32] has been recognized as a very useful means of predicting the true appearance of the source Fig. 26.2. (The near-field effect on resolution was first introduced in the field of microwaves [26.33].) The basis of this method is to include or measure exponentially decaying waves as they propagate from the sound source so that the sources can be completely reconstructed.

Another class of approaches are based on the parametric method, which derives its name from the fact that the signal is modeled using certain parameters. In other words, the basis function is chosen depending upon the prediction of the sound source. A typical method of this kind is the so-called *beam-forming method*. Different types of basis functions can be chosen for this method, entirely depending on the sound field that the basis function is trying to map [26.34, 35]. In Fig. 26.1, we can select either the elephants or dogs (or another choice), depending on what we want to predict. This type of mapping gives information about the source location. As illustrated in Fig. 26.1, the basis function maps the signal by changing its parameter; in the case of forming a plane-wave beam, the incident angle of the plane wave can be regarded as a parameter. The main issues that have been discussed for this kind of mapping method

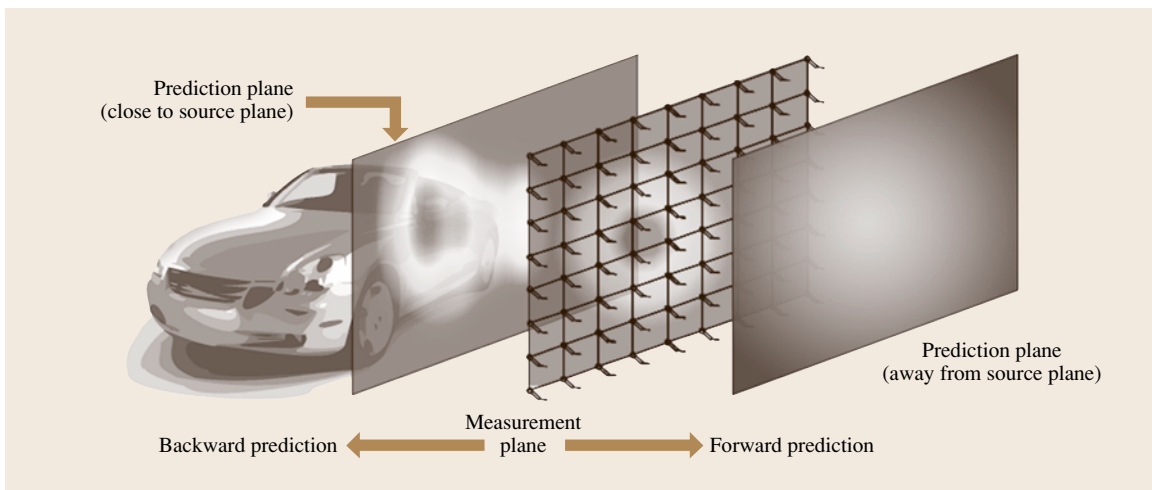


Fig. 26.2 Illustration of acoustic holography. Near-field acoustic holography measures evanescent waves on the measurement plane. The measurement plane is always finite, i. e. there is always a finite aperture. Therefore, we only get limited data

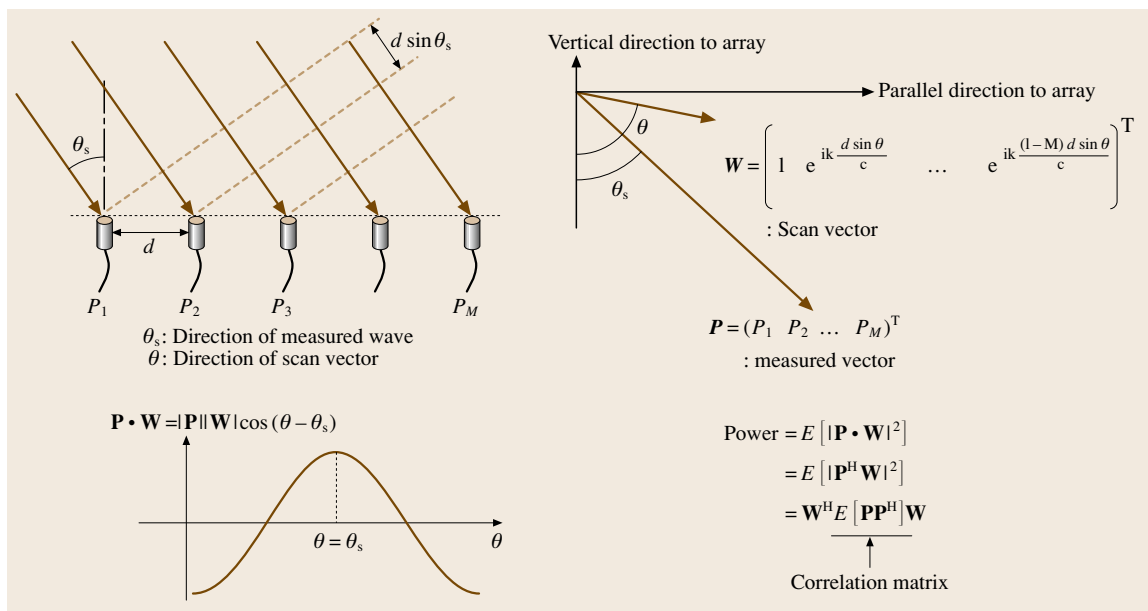


Fig. 26.3 The beam-forming method

are directly related to the structure of the correlation matrix that comes from the measured acoustic pressure vector and its complex conjugate (see Fig. 26.3 for the details). In this method, each scan vector has a multiplicative parameter; for the plane wave in Fig. 26.3 it is the angle of arrival. The correlation matrix is given as illustrated in Fig. 26.3. The scan vector is a basis function in this case. As one can see immediately, this problem is directly related to the structure of the correlation matrix and the basis function used. The signal-to-noise (S/N) ratio of the measured correlation matrix determines the effectiveness of the estimation. There have been many attempts to improve the estimator's performance with

regard to the signal-to-noise ratio [26.35, 36]. These methods have mainly been developed for applications in the radar and underwater communities [26.37]. This technique has also been applied to a noise source location finding problem; high-speed-train noise source estimation [26.38–40] is one such example. Various shapes of arrays have been tried to improve the spatial resolution [26.41–43]. However, it is obvious that these methods cannot sense the shape of the sound or noise source; they only provide its location. Therefore, we will not discuss the beam-forming method in this chapter. In the next section, the problems that we have discussed will be defined.

26.2 Acoustic Holography: Measurement, Prediction and Analysis

26.2.1 Introduction and Problem Definitions

Acoustic holography consists of three components: measurement, which consists of measuring the sound pressure on the hologram plane, prediction of the acoustic variables, including the velocity distribution, on the plane of interest, and analysis of the holographic reconstruction. This last component was not recognized as important as the others in the past. However, it yields the real meaning of the sound picture: visualization.

The issues associated with measurement are all related to the hologram measurement configuration; we measure the sound pressure at discrete measurement points over a finite measurement area (finite aperture), as illustrated in Fig. 26.2. References [26.44–52] explain the necessary steps to avoid spatial aliasing, wrap-around errors, and the effect of including evanescent waves on the resolution (near-field acoustic holography). If sensors are incorrectly located on the hologram surface, errors result in the prediction results. Similar errors can be produced when there is a mag-

nitude and phase mismatch between sensors. This is well summarized in [26.53]. There have been many attempts to reduce the aperture effect. One method is to extrapolate the pressure data based on the measurements taken [26.50, 52]. Another method allows the measurement of sound pressure in a sequence and interprets the measured sound pressures with respect to reference signals, assuming that the measured sound pressure field is stationary during the measurement and the number of independent sources is smaller than the number of reference microphones [26.54–61]. Another method allows scanning or moving of the microphone array, thereby extending the aperture size as much as possible [26.62–65]. This also allows one to measure the sound pressure generated by moving sound sources, such as a vehicle's exterior noise.

The prediction problem is rather well defined and relatively straightforward. Basically, the solution of the acoustic wave equation usually results in the sound pressure distribution on the measurement plane. Prediction can be attempted using a Green's function, an example of which may be found in the Kirchhoff–Helmholtz integral equation. It is noteworthy, however, that the prediction depends on the shape of the measurement and prediction surfaces, and also on the presence of sound reflections [26.54, 66–87].

The acoustic holography analysis problem was introduced rather recently. As mentioned earlier in this section, this is one of the essential issues connected to the general inverse problem. One basic question is whether what we see and imagine is related to what happens in reality. There are two different sound/noise sources, one of which is really radiating the sound, and the another that is reflecting the sound. The former is of-

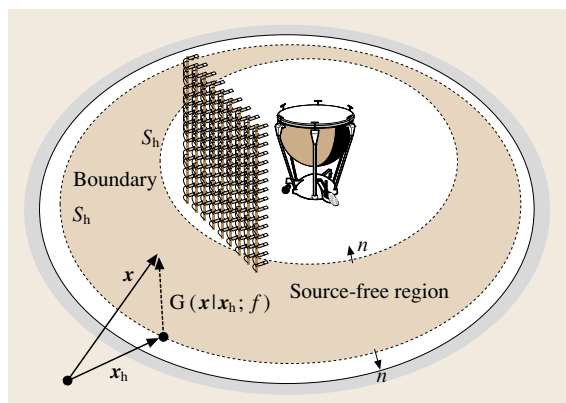


Fig. 26.4 The geometry and nomenclature for the Kirchhoff–Helmholtz integral (26.1)

ten called *active sound/noise*, while the latter is called *passive sound/noise*. This is an important practical concept for establishing noise control strategies; we want to eliminate the active noise source. Another concern is whether the sources are independently or dependently correlated (Fig. 26.23). The concept of an independent and dependent source has to be addressed properly to understand the issues.

26.2.2 Prediction Process

The prediction process is related to how we predict the unmeasured sound pressure or other acoustic variables based on the measured sound pressure information. The following equation relates the unmeasured and measured pressure

$$P(x; f) = \int_{S_h} \left[G(x|x_h; f) \frac{\partial P}{\partial n} \Big|_{(x=x_h; f)} - P(x_h; f) \frac{\partial G(x|x_h; f)}{\partial n} \right] dS_h. \quad (26.1)$$

Equation (26.1) is the well-known Kirchhoff–Helmholtz integral equation, where $G(x|x_h; f)$ is the free-space Green's function. This equation essentially says that we can predict the sound pressure anywhere if we know the sound pressures and velocities on the boundary Fig. 26.4. However, it is noteworthy that measuring the velocity on the boundary is more difficult than measuring the sound pressure. This rather practical difficulty can be solved by introducing a Green's function that

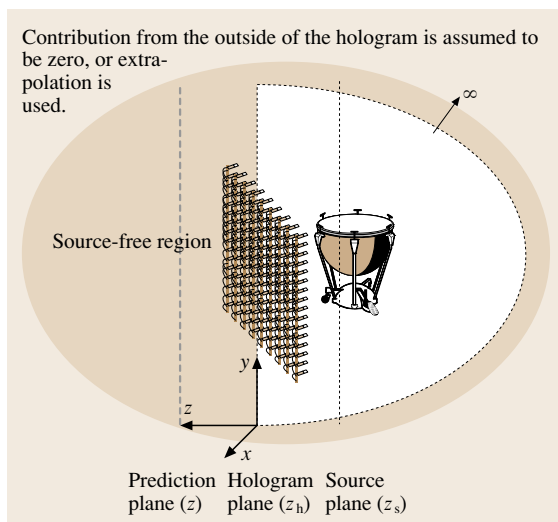


Fig. 26.5 Illustration of the planar acoustic holography

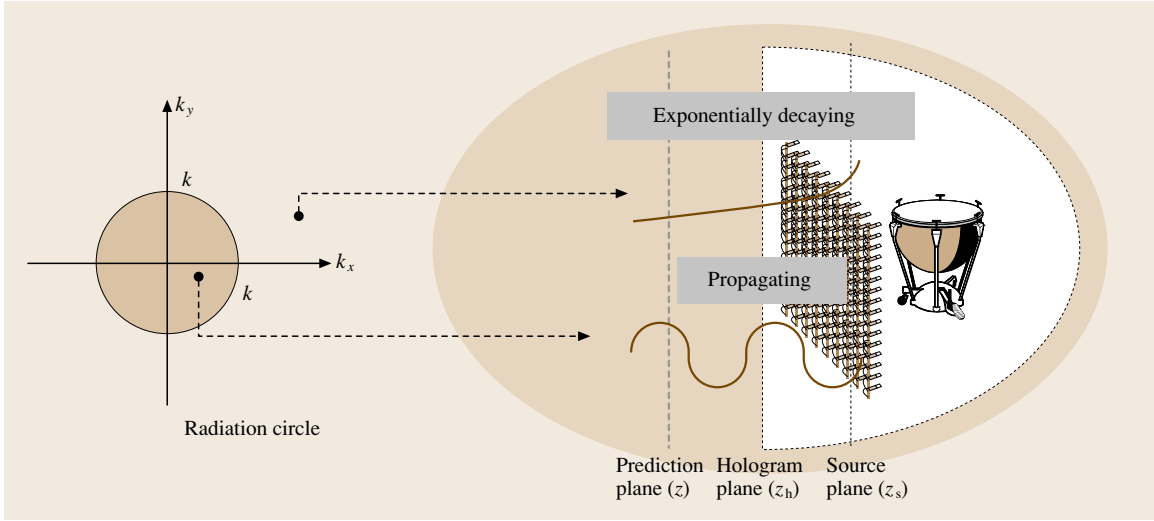


Fig. 26.6 Propagating and exponentially waves in acoustic holography

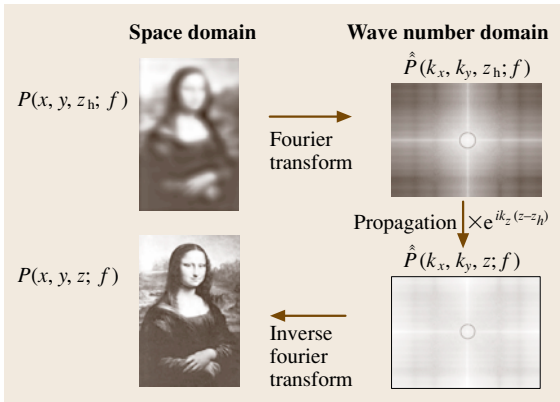


Fig. 26.7 The data-processing procedure for acoustic holography

satisfies the Dirichlet boundary condition: $G_D(\mathbf{x}|\mathbf{x}_h; f)$. Then, (26.1) becomes

$$P(\mathbf{x}; f) = \int_{S_h} \left[-P(\mathbf{x}_h; f) \frac{\partial G_D(\mathbf{x}|\mathbf{x}_h; f)}{\partial n} \right] dS_h. \quad (26.2)$$

This equation allows us to predict the sound pressure on any surface of interest. It is noteworthy that we can choose a Green's function as long as it satisfies the linear inhomogeneous wave equation, or the inhomogeneous Helmholtz equation in the frequency domain. That is,

$$\nabla^2 G(\mathbf{x}|\mathbf{x}_h; f) + k^2 G(\mathbf{x}|\mathbf{x}_h; f) = -\delta(\mathbf{x} - \mathbf{x}_h). \quad (26.3)$$

Therefore, we can select a Green's function in such a way that we can eliminate one of the terms on the right-hand side of (26.1); (26.2) is one such case.

To see what essentially happens in the prediction process, let us consider (26.2) when the measurement and prediction plane are both planar. Planar acoustic holography assumes that the sound field is free from reflection (Fig. 26.5); then we can write (26.2) as

$$P(x, y, z; f) = \int_{S_h} P(x_h, y_h, z_h; f) \times K_{PP}(x - x_h, y - y_h, z - z_h; f) dS_h, \quad (26.4)$$

$$K_{PP}(x, y, z; f) = \frac{1}{2\pi} \frac{z}{r^3} (1 - ikr) \exp(ikr), \quad (26.5)$$

$$\text{where } r = \sqrt{x^2 + y^2 + z^2},$$

$$k = \frac{2\pi f}{c},$$

$$\mathbf{x} = (x, y, z),$$

$$\mathbf{x}_h = (x_h, y_h, z_h).$$

K_{PP} can be readily obtained by using two free-field Green's functions that are located at z_h and $-z_h$, so that it satisfies the Dirichlet boundary condition.

This is a convolution integral, and therefore we can write this in the wave-number domain as

$$\begin{aligned} & \hat{P}(k_x, k_y, z; f) \\ &= \hat{P}(k_x, k_y, z_h; f) \exp[ik_z(z - z_h)], \end{aligned} \quad (26.6)$$

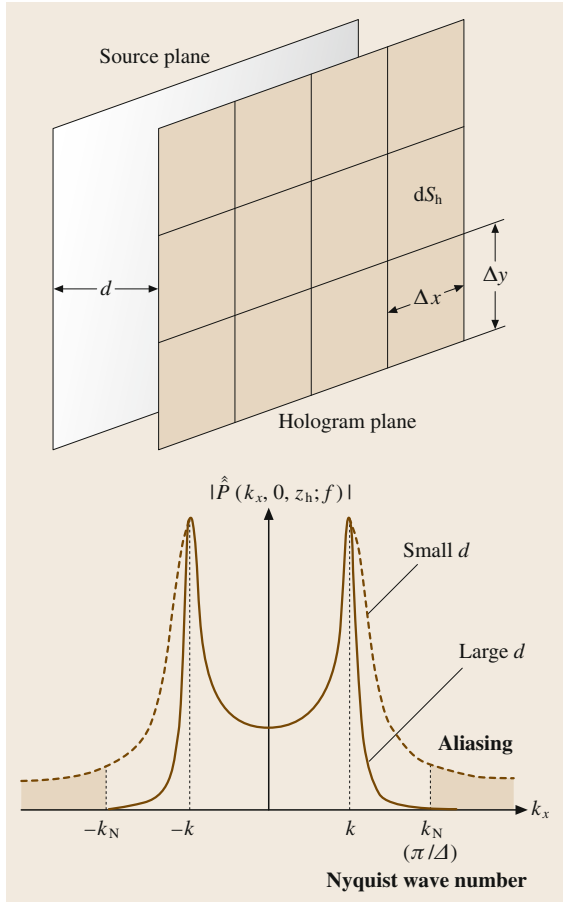


Fig. 26.8 The error due to discrete measurement: the spatial aliasing problem. The microphone spacing determines the Nyquist wave number. This wave number has to be smaller than the maximum wave number of the acoustic pressure distribution on the hologram plane. The microphone spacing, therefore, has to get smaller as the distance between the hologram (the measurement plane) and source decrease. The rule of thumb is $\delta < d$ ◀

where

$$\hat{P}(k_x, k_y, z; f) = \int_{-\infty}^{\infty} \int_{-\infty}^{\infty} P(x, y, z; f) e^{-i(k_x x + k_y y)} dx dy, \quad (26.7)$$

$$k_z = \sqrt{k^2 - k_x^2 - k_y^2}.$$

This equation essentially predicts the sound pressure with respect to the wave number (k_x, k_y) . If $k^2 \geq k_x^2 + k_y^2$, the wave in z -direction (k_z) is propagating in space. Otherwise, the z -direction wave decays exponentially, i. e. it is an evanescent wave (Fig. 26.6).

We have derived the formulas that can predict what we did not measure based on what we measured, by using a Green's function. It is noteworthy that we can get the same results if we use the characteristic solutions of the Helmholtz equation; the Appendix describes the details. The Appendix also includes discrete expressions for the formula, which are normally used in the computation.

Equation (26.6) also allows us to predict the sound pressure on the source plane, when $z = z_s$. This is an inverse problem because it predicts the pressure distribution on the source plane based on the hologram pressure (Figs. 26.3 and 26.6).

Figure 26.7 essentially illustrates how we can process the data for predicting what we did not measure based on what we measure. There are four major areas that cause errors in acoustic holography prediction. One is related to the integration of (26.4). Equation (26.4) has to be implemented on the discretized surface Fig. 26.8. This surface, therefore, has to be spatially sampled according to the selected surface. This spatial sampling can produce spatial aliasing, depending on the spatial distribution of the sound source; the sampling wave number must be larger than twice the maximum wave number of interest. It is noteworthy that, as illustrated in Fig. 26.8, the distance between the

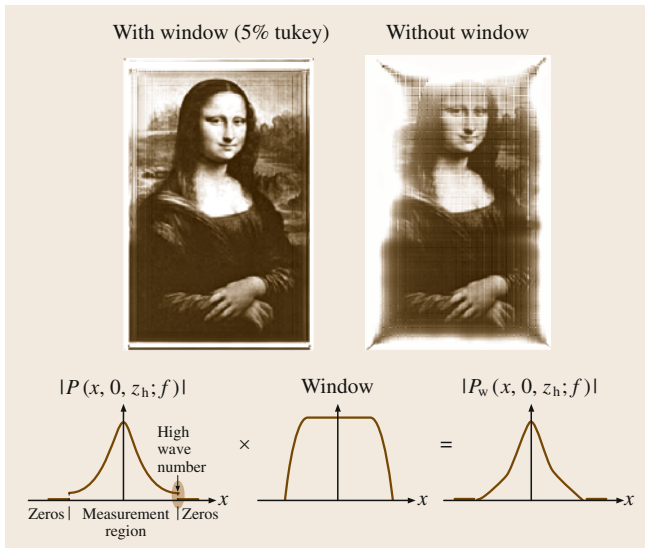


Fig. 26.9 The effect of a finite aperture: the rapid change at the aperture edges produces high-wave-number noise ◀

hologram and source planes is usually related to the sampling distance d . The closer one is to the source, the smaller the sampling distance needs to be. We must also note that the size of the aperture determines the wave-number resolution of acoustic holography. The finite aperture inevitably produces very sharp data truncation, as illustrated in Fig. 26.9. This produces unrealistic high-wave-number noise (see *without window* in Fig. 26.9). Therefore, it is often required that we use a window, which can result in a smoother data transition from what is on the measurement plane to what is not measured (Fig. 26.9).

The spatial Fourier transform that has to be done in the prediction process (26.6) has to be carried out in the domain for which data is available, i.e. a finite Fourier transform. It therefore produces a ghost hologram, as illustrated in Fig. 26.10 [26.46, 50]. This effect can be effectively removed by adding zeros to the hologram data (Fig. 26.11). The last thing to note is what can happen when we do backward propagation. As we can see in (26.6), when we predict the sound pressure distribution on a plane close to the sound source ($z < z_h$) (Fig. 26.5)) and k_z has an imaginary value (evanescent wave), then the sound pressure distribution of the exponentially decaying part will be unrealistically magnified (Fig. 26.11) [26.47]. Figure 26.12 graphically summarizes the entire processing steps of acoustic holography.

The issues related with the evanescent wave and its measurement are well addressed in the literature [26.88]. The measurement of evanescent waves essentially allows us to achieve higher resolution than conventional acoustic holography [26.89–94]. However, it is noteworthy that the evanescent-wave component is substantially smaller than the other propagating components. Therefore, it is easy to produce errors that are associated with sensor or position mismatch [26.53]; in other words, it is very sensitive to the signal-to-noise ratio. Errors due to position and sensor mismatch are bias errors and random errors, respectively. It has been shown [26.53] that the bias error due to the mismatches is negligible, but the random error is significant in backward prediction. This is related to the measurement spacing on the hologram plane (Δ_h), prediction plane (Δ_z), and the distance between the hologram plane and the prediction plane (d). It is approximately proportional to $24.9(d/\Delta_z) + 20 \log_{10}(\Delta_h/\Delta_z)$ in a dB scale. The signal-to-noise ratio can be amplified when we try to reconstruct the source field: a typical ill-posed phenomena. There have been many attempts to reduce this effect by using a spatial filter [26.47, 95–99], which is often called the *regularization* of acoustic holography [26.100–115].

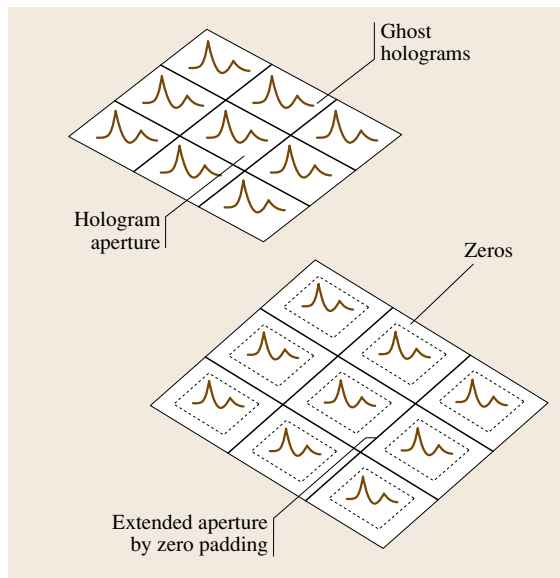


Fig. 26.10 The effect of the finite spatial Fourier transform on acoustic holography: the ghost image is due to the finite Fourier transform; circular convolution can be eliminated by adding zeros

Depending on the separable coordinates that we use for acoustic holography, we can construct cylindrical or spherical coordinates [26.54, 67, 69] (Figs. 26.13 and

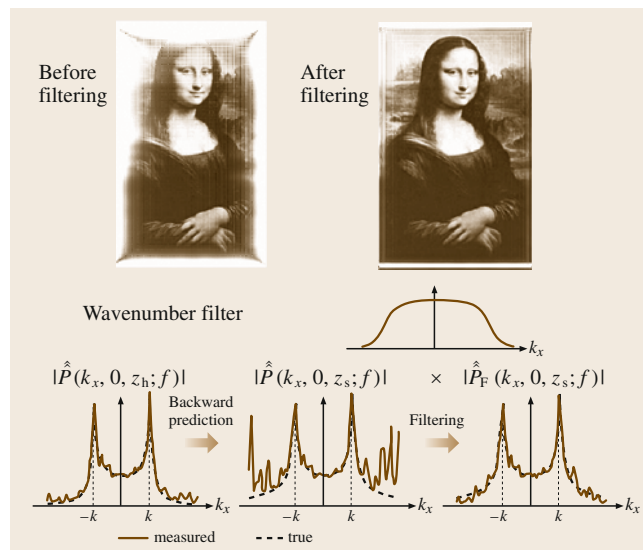


Fig. 26.11 Wave-number filtering in backward prediction. Evanescent wave components are magnified without filtering (after [26.47])

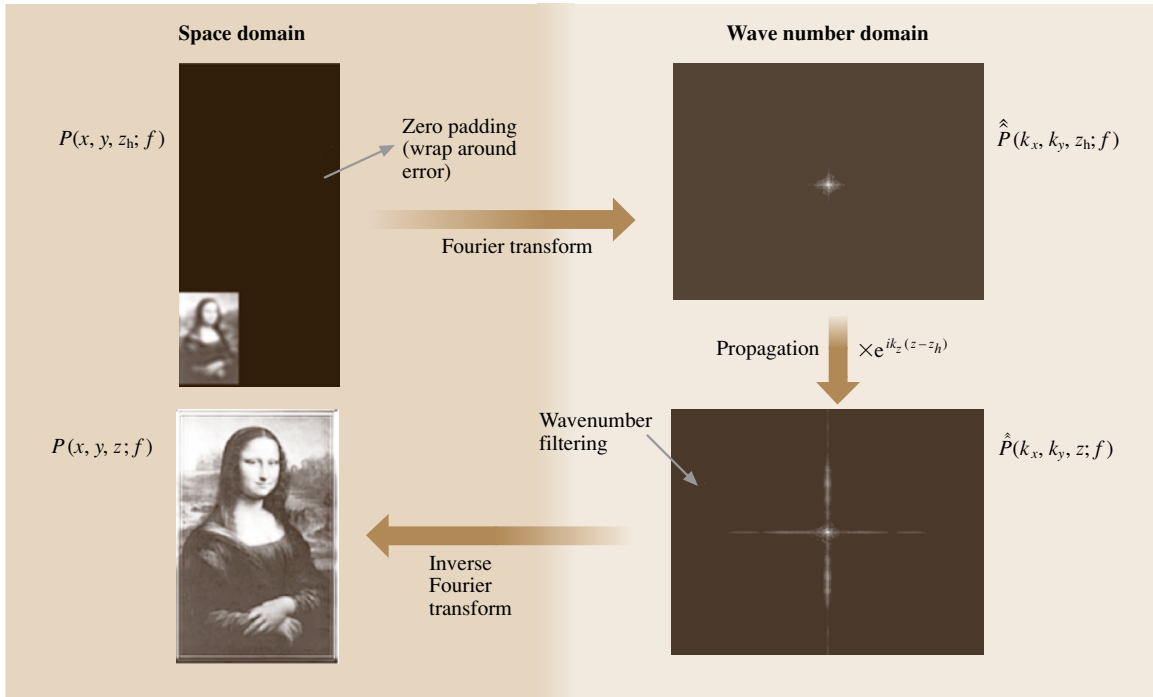


Fig. 26.12 Summary of the acoustic holography prediction process

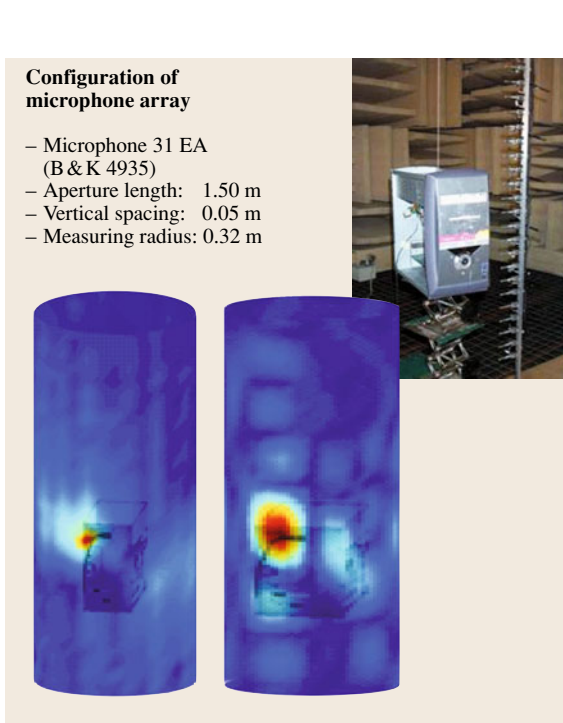


Fig. 26.13 Cylindrical holography

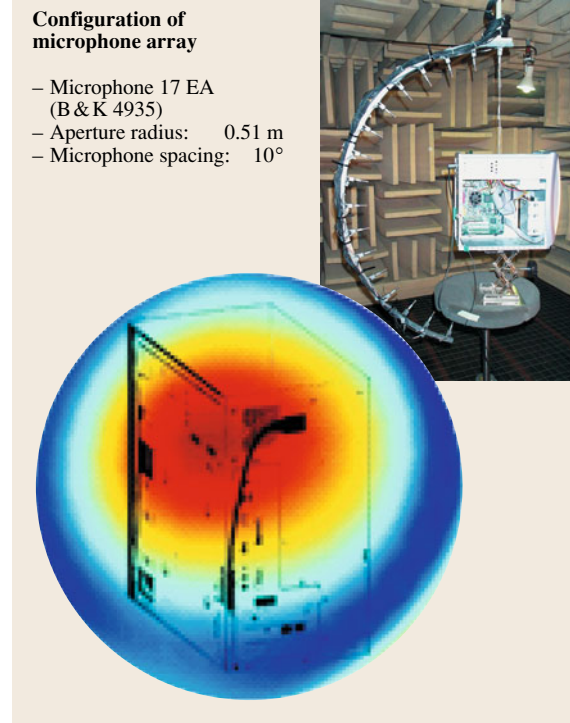


Fig. 26.14 Spherical holography

26.14). These methods predict the sound field in exactly the same manner as in planar holography but with respect to different coordinates. As expected, however, these methods have some advantages. For example, the wrap-around error is negligible – in fact, there is no such error in spherical acoustic holography – and there is no aperture-related error [26.54]. Recently, the advantage of using spherical functions has also been noted [26.79, 81, 86, 87, 113].

26.2.3 Measurement

To construct a hologram, we commonly measure the sound pressure at discrete positions, as illustrated in Fig. 26.2. However, if the sound generated by the source, and therefore the sound field, can be assumed

to be stationary, then we do not have to measure them at the same time.

Figure 26.15 illustrates one way to accomplish this measurement. This method normally measures the sound pressure field using a stepped line array (Fig. 26.15a). To understand the issues associated with this measurement system for the sake of its simplicity, let us see how we process a signal of frequency f when there is a single source. The relationship between the sound source and sound pressure in the field, or measurement position (x_h), can be written as

$$P(x_h; f) = H(x_h; f)Q(f), \quad (26.8)$$

where $Q(f)$ is the source input signal and $H(x_h; f)$ is the transfer function between the source input and the measured pressure. This means that, if we know the transfer function and the input, we can find the magnitude and phase between the measured positions. Because it is usually not practical to measure the input, we normally use reference signals (Fig. 26.15a). By using a reference signal, the pressure can be written as

$$P(x_h; f) = H'(x_h; f)R(f), \quad (26.9)$$

where $R(f)$ is the reference signal. We can obtain $H'(x_h; f)$ by

$$H'(x_h; f) = \frac{P(x_h; f)}{R(f)}. \quad (26.10)$$

The input and reference are related through

$$R(f) = H_R(f)Q(f), \quad (26.11)$$

where $H_R(f)$ is the transfer function between the input and the reference. As a result, we can see that (26.9) has the same form as (26.8).

It is noteworthy that (26.8) holds for the case that we have only one sound source and the sound field is stationary and random. However, if there are two sound sources, then (26.8) becomes

$$P(x_h; f) = H_1(x_h; f)Q_1(f) + H_2(x_h; f)Q_2(f), \quad (26.12)$$

where $Q_i(f)$ is the i -th input and $H_i(x_h; f)$ is its transfer function. There are now two independent sound fields. This requires, of course, two independent reference signals. It has been well accepted that the number of reference microphones has to be greater than the number of independent sources [26.57]. However, if this is strictly true, then it means that we have to somehow know the number of sources, and this, in some degree, contradicts the the acoustic holography approach.

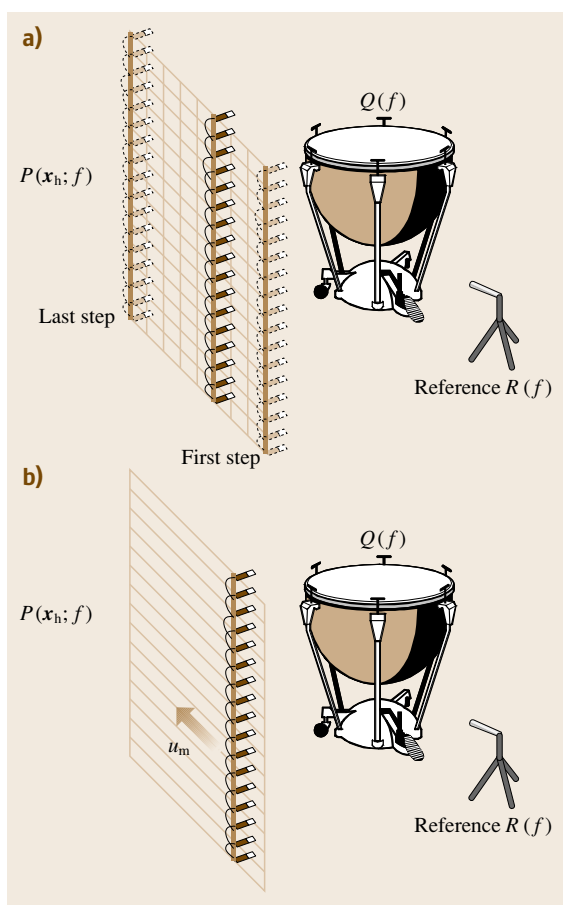


Fig. 26.15a,b Two measurement methods for the pressure on the hologram plane: (a) step-by-step scanning (b) continuous scanning

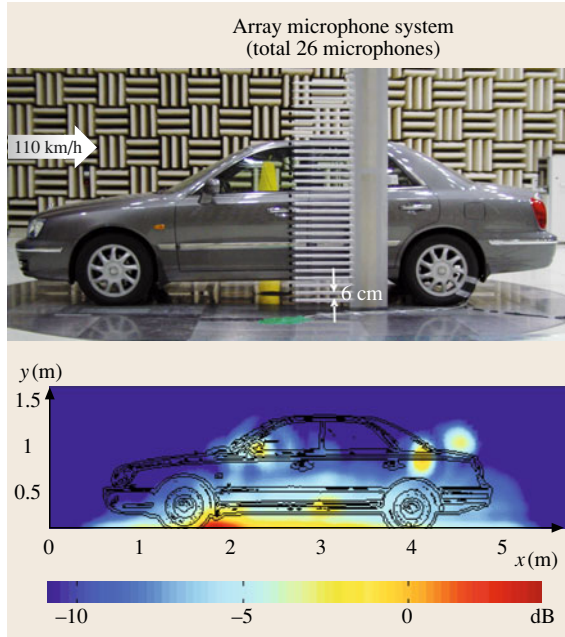


Fig. 26.16 Application result of the step-by-step scanning method to the wind noise of a car. This figure is the pressure distribution at 710 ~ 900 Hz in a source plane when the flow velocity is 110 km/h. In this experiment, 17 reference microphones are randomly located in the car, to see the coherence between interior noise and what are measured by the array microphone system. The array microphone system was initially located at 3 m forward from the middle point of a car, and moved 6 cm in step until it reached at 3 m backward from the middle point ◀

Figure 26.16 shows an example of this method when there are many independent sound fields. On the other hand, one study showed that we can even continuously scan the sound field by using a line array of microphones (Fig. 26.15b) [26.62–65]. This method essentially allows us to extend the aperture size without any limit as long as the sound field is stationary. In fact, [26.65] also showed that this method can be used for a slowly varying (quasi-stationary) sound field.

A recent study [26.61] demonstrated that the measured information, the location of the sources, and the number of independent sources converge to their true values as the number of reference microphones increases. This study also showed that high-power sources are likely to be identified even if the number of reference microphones is less than the number of sources.

This method has to deal with the Doppler shift. For example, let us consider a plane wave in the $(k_{x_0}, k_{y_0}, k_{z_0})$ direction and a pure tone of frequency f_{h_0} . Then the pressure on the hologram plane can be written as

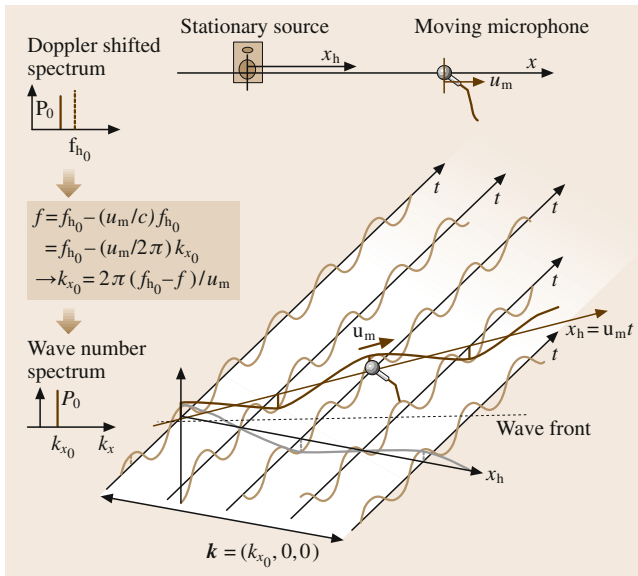
$$p(x_h, y_h, z_h; t) = P_0 \exp [i(k_{x_0}x_h + k_{y_0}y_h + k_{z_0}z_h)] \exp(-i, f_{h_0}t), \quad (26.13)$$

where P_0 denotes the complex magnitude of the plane wave. Spatial information about the plane wave with respect to the x -direction can be represented by a wave-number spectrum, and can be described as

$$\begin{aligned} \hat{P}(k_x, y_h, z_h; t) &= \int_{-\infty}^{\infty} p(x_h, y_h, z_h; t) e^{-ik_x x_h} dx_h \\ &= P_0 \exp [i(k_{y_0}y_h + k_{z_0}z_h)] \\ &\quad \times \delta(k_x - k_{x_0}) \exp(-i2\pi f_{h_0}t) \\ &= P(k_{x_0}, y_h, z_h) \delta(k_x - k_{x_0}) \\ &\quad \times \exp(-i2\pi f_{h_0}t), \end{aligned} \quad (26.14)$$

where $P(k_{x_0}, y_h, z_h) = P_0 \exp[i(k_{y_0}y_h + k_{z_0}z_h)]$ is the wave-number spectrum of the plane wave at $k_x = k_{x_0}$.

Fig. 26.17 The continuous scanning method for a plane wave and a pure tone (one-dimensional illustration). f_{h_0} is the source frequency, f is the measured frequency, u_m is the microphone velocity, c is the wave speed, k_{x_0} is the x -direction wave number, and P_0 is the complex amplitude of a plane wave ◀



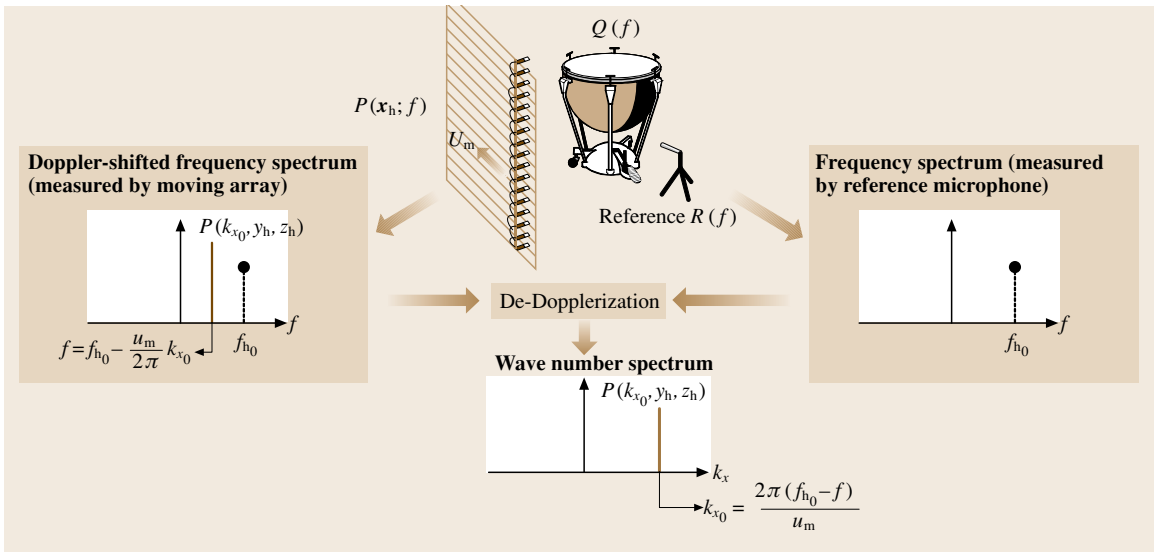


Fig. 26.18 De-Dopplerization procedure for a line spectrum

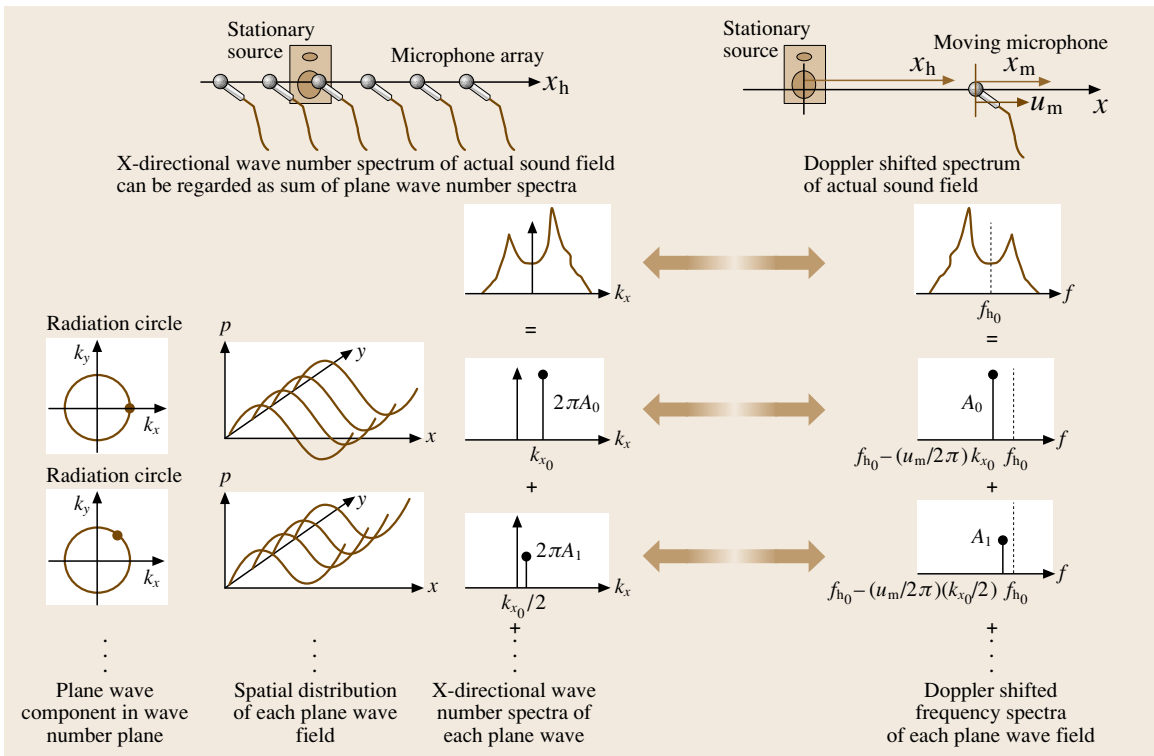


Fig. 26.19 The continuous scanning method for a more general case (one-dimensional illustration)

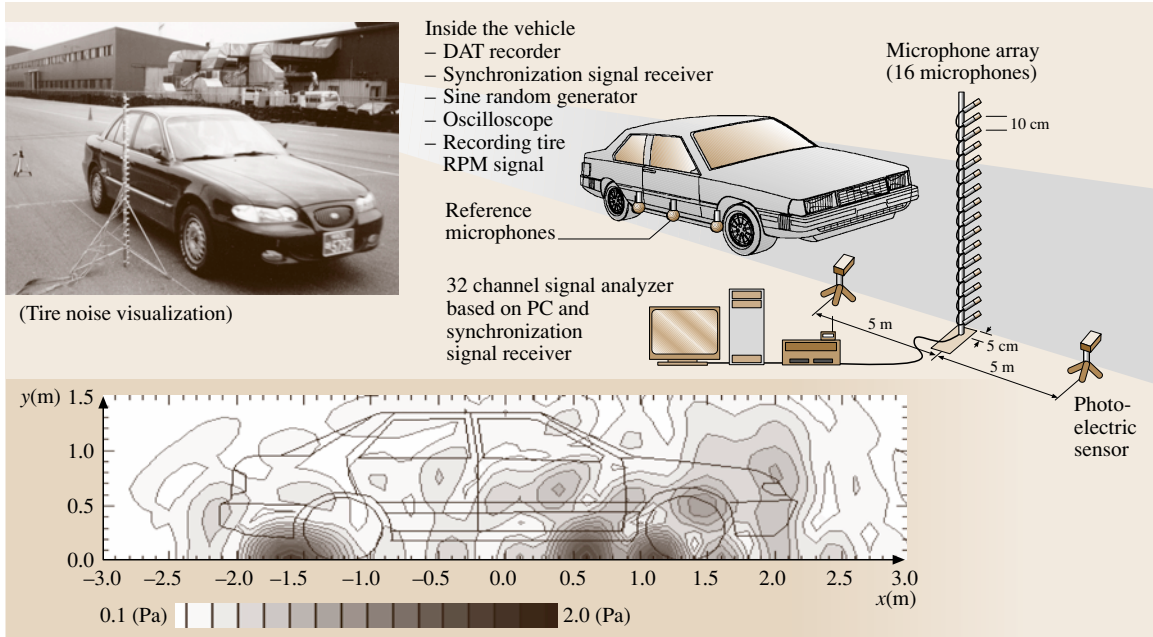


Fig. 26.20 Experimental configuration and result of the continuous scanning method to vehicle pass-by noise. The tire pattern noise distribution (pressure) on the source plane is shown when the car passed the microphone array with constant speed of 50 km/h

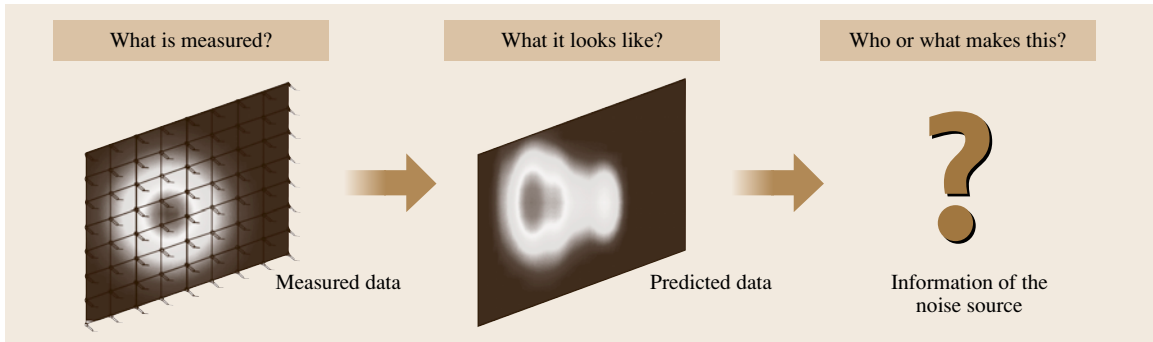


Fig. 26.21 Illustration of analysis problem in acoustic holography

If a microphone is moving at an x -velocity u_m , the measured signal $p_m(x_h, y_h, z_h; t)$ is

$$p_m(x_h, y_h, z_h; t) = p(u_m t, y_h, z_h; t). \quad (26.15)$$

The Fourier transform of (26.15) with respect to time F_T , using (26.13), can be expressed as

$$F_T[p_m(u_m t, y_h, z_h; t)] = \int_{-\infty}^{\infty} p_m(u_m t, y_h, z_h; t) e^{i2\pi f t} dt$$

$$= P_0 \exp[i(k_{y_0} y_h + k_{z_0} z_h)] \times \delta\left(\frac{u_m}{2\pi} k_{x_0} - f_{h_0} + f\right) = P(k_{x_0}, y_h, z_h) \delta\left(\frac{u_m}{2\pi} k_{x_0} - f_{h_0} + f\right). \quad (26.16)$$

Equation (26.16) means that the complex amplitude of the plane wave is located at the shifted frequency $f_{h_0} - u_m k_{x_0} / 2\pi$, as shown in Fig. 26.17. In general, the relation between the shifted frequency f and x -direction wave number k_x is expressed as

Fig. 26.18

$$k_x = \frac{2\pi(f_{h0} - f)}{u_m} \quad (26.17)$$

We can measure the original frequency f_{h0} by a fixed reference microphone. Using the Doppler shift, we can therefore obtain the wave-number components from the frequency components of the moving microphone signal. Figure 26.19 illustrates how we obtain the wave-number spectrum.

This method essentially uses the relative coordinate between the hologram and microphone. Therefore, it can be used for measuring a hologram of moving noise sources (Fig. 26.20), which is one of the major contributions of this method [26.62–65].

26.2.4 Analysis of Acoustic Holography

Once we have a picture of the sound (acoustic holography), the questions about its meaning are the next topic of interest. What we have is usually a contour plot of the sound pressure distribution or a vector plot of the sound intensity on a plane of interest. This plot may help us to imagine where the sound source is and how it radiates into space with respect to a frequency of interest. However, in the strict sense, the only thing we can do from the two-dimensional expression of sound pressure or intensity distribution is to guess what was really there. We do not know, precisely, where the sound sources are (Fig. 26.21).

As mentioned earlier, there are two types of sound sources: active and passive sound source. The former is the source that radiates sound itself, while the latter only radiates reflected sound. These two different types of sound sources can be distinguished by eliminating reflected sound [26.116]. This is directly related to the way boundary conditions are treated in the analysis.

The boundary condition for a locally reacting surface can be written as [26.116–118]

$$V(\mathbf{x}_s; f) = A(\mathbf{x}_s; f)P(\mathbf{x}_s; f) + S(\mathbf{x}_s; f), \quad (26.18)$$

where $V(\mathbf{x}_s; f)$ and $P(\mathbf{x}_s; f)$ are the velocity and pressure on the wall. $A(\mathbf{x}_s; f)$ is the wall admittance and $S(\mathbf{x}_s; f)$ is the source strength on the wall. The active sound source is located at a position such that the source strength is not zero. This equation says that we can estimate the source strength if we measure the wall admittance. To do this, it is necessary to first turn off the source or sources, and then measure the wall admittance by putting a known source in the desired position (Fig. 26.22a). The next step is to turn on the

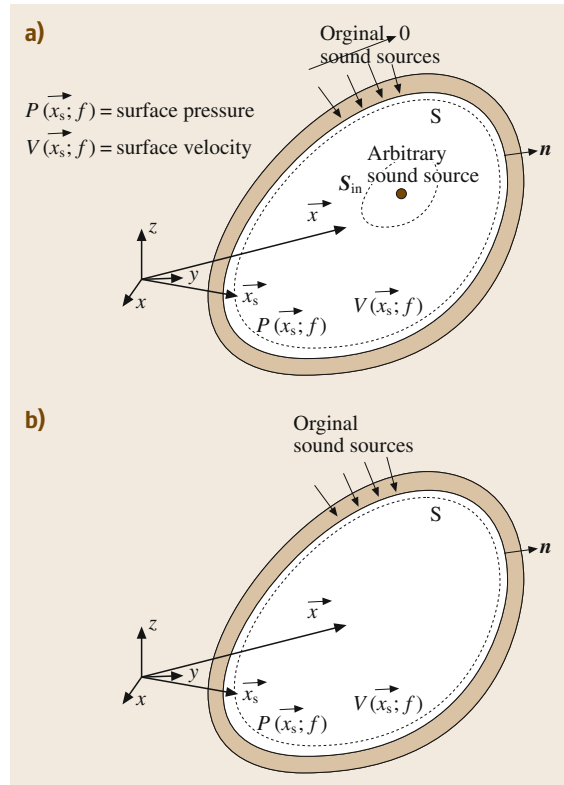


Fig. 26.22a,b Two steps to separate the active and passive source: (a) Admittance measurement, (b) source strength measurement

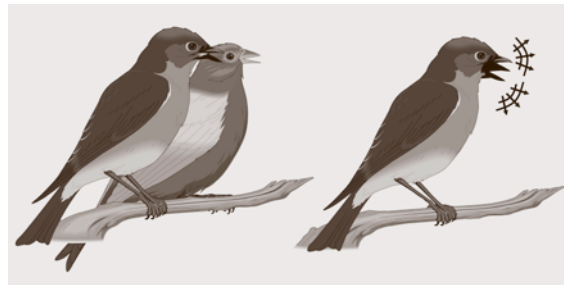


Fig. 26.23 Spatially independent or dependent sources

sources and obtain the sound pressure and velocity distribution on the wall, using the admittance information (Fig. 26.22b). This provides us with the location and strength of the source (i.e. the source power; for example, see Fig. 26.24).

Another very important problem is whether or not we can distinguish between independent or dependent sources, i.e. two birds singing versus one bird with two

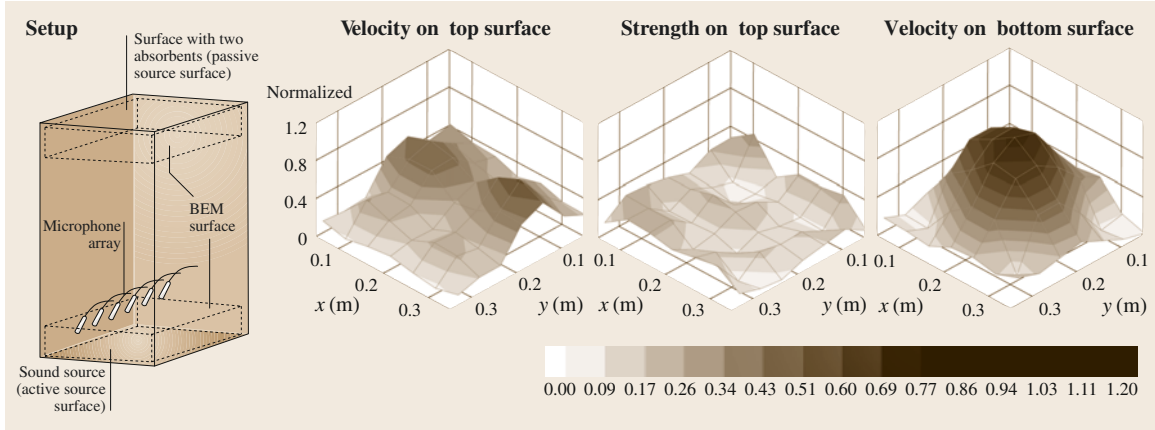


Fig. 26.24 Experiment results that separate the active and passive sources. The top surface is made by the sound absorption material. The speaker on the bottom surface, which is reflecting sound, is eliminated by this separation

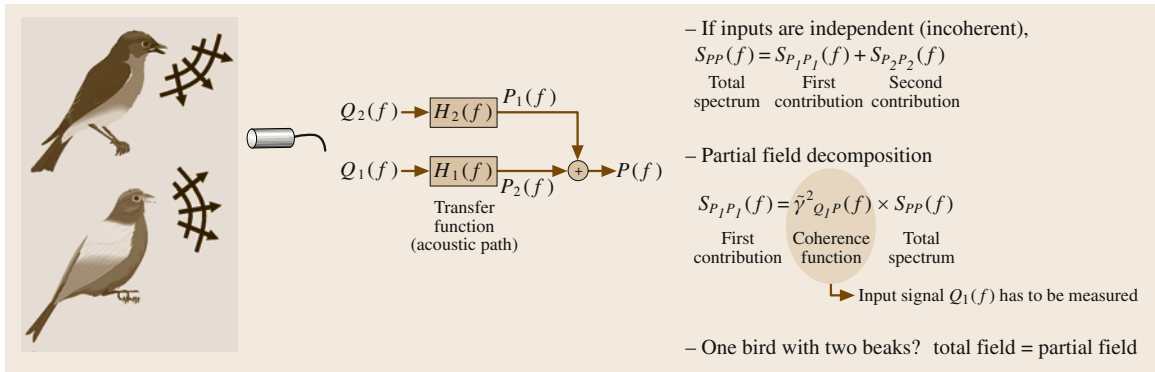


Fig. 26.25 A two-input single-output system and its partial field

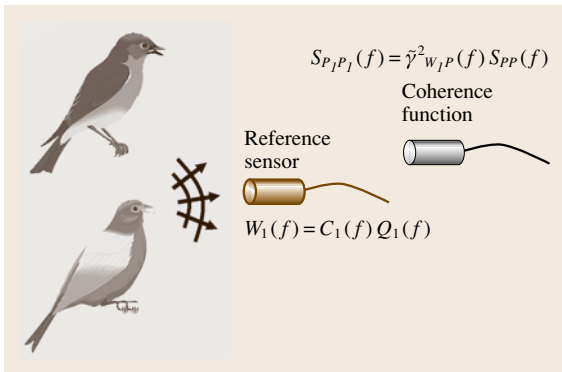


Fig. 26.26 The conventional method to obtain the partial field

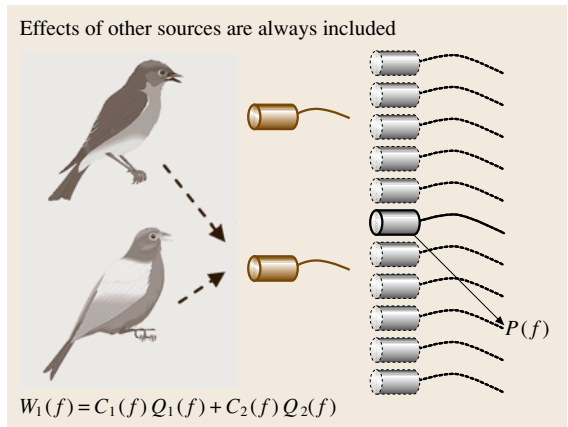


Fig. 26.27 Acoustic holography and partial field decomposition

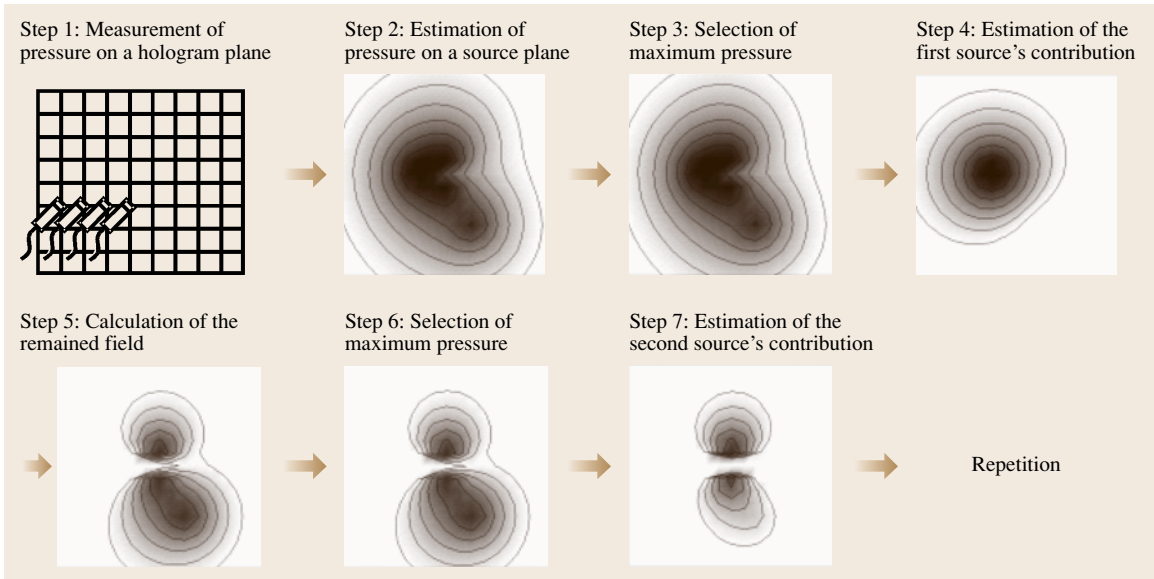


Fig. 26.28 The procedure to separate the independent and dependent sources

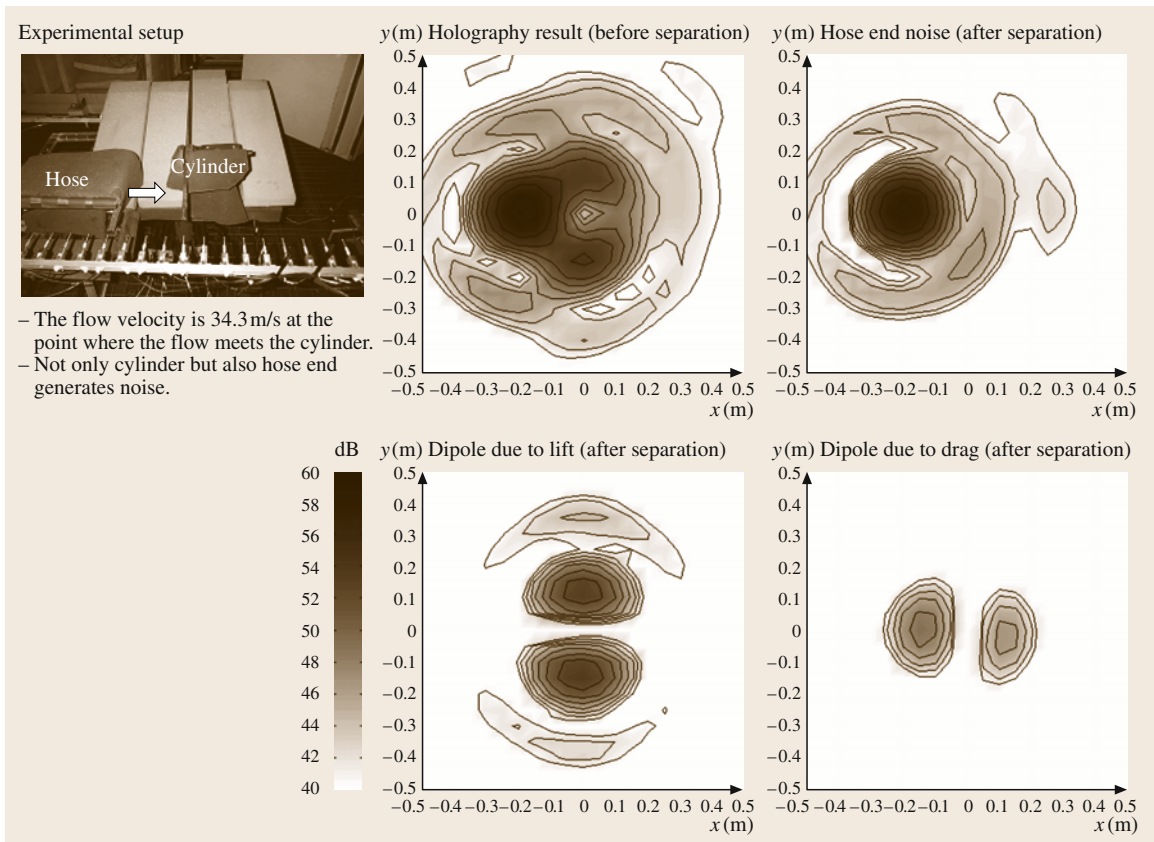


Fig. 26.29 The separation method applied to a vortex experiment

beaks (Fig. 26.23). This has a rather significant practical application. For example, to control noise sources effectively, we only need to control independent noise sources. This can be achieved by using the statistical differences between signals that are induced by independent and dependent sound sources.

For example, let us consider a two-input single-output system (Fig. 26.25). If the two inputs are independent, the spectrum $S_{PP}(f)$ of the output $P(f)$ can be expressed as

$$S_{PP}(f) = |H_1(f)|^2 S_{Q_1 Q_1}(f) + |H_2(f)|^2 S_{Q_2 Q_2}(f), \quad (26.19)$$

where $S_{Q_i Q_i}(f)$ is the spectrum of the i -th input $Q_i(f)$, and $H_i(f)$ is its transfer function. The first and second terms represent the contributions of the first and second input to the output spectrum, respectively. If we can obtain a signal as

$$W_1(f) = C(f)Q_1(f), \quad (26.20)$$

then we can estimate the contribution of the first source as [26.119]

$$S_{P_1 P_1}(f) = |H_1(f)|^2 S_{Q_1 Q_1}(f) = \gamma_{W_1 P}^2(f) S_{PP}(f), \quad (26.21)$$

where $\gamma_{W_1 P}^2(f)$ is the coherence function between $W_1(f)$ and $Q_1(f)$ (Fig. 26.26).

We can simply extend (26.21) to the case of multiple outputs, as in the case of acoustic holography (Fig. 26.27). The main problem is how to obtain a signal that satisfies (26.20). We can generally say that, by putting sensors closer to the source or sources [26.57, 58, 120–123], we may have a better signal that can be used to distinguish between independent or dependent sources. However, this is neither well proven nor practical, as it is not always easy to put the sensors close to the sources. Very recently, a method that does not require this [26.124, 125] was developed. Figure 26.28 explains the method's procedures. The first and second steps are the same as in acoustic holography: measurement and prediction. The third step is to search for the maximum pressure on the source plane. This method assumes that the maximum pressure satisfies (26.20). The fourth step is to estimate the contribution of the first source by using the coherence functions between the maximum pressure and other points, as in (26.21). The fifth step is to calculate the remaining spectrum by subtracting the first contribution from the output spectrum. These steps are repeated until the contributions of the other sources are estimated (Fig. 26.29).

26.3 Summary

As expected, it is not simple to answer the question of whether we can see the sound field. However, it is now understood that the analysis of what we obtained, acoustic holography, needs to be properly addressed, although little attention was given to this problem in the past. We now understand better how to obtain informa-

tion from the sound picture. Making a picture is the job of acoustic holography, but the interpretation of this picture is the responsibility of the observer. This paper has reviewed some useful guidelines for better interpretation of the sound field to deduce the right impression or information from the picture.

26.A Mathematical Derivations of Three Acoustic Holography Methods and Their Discrete Forms

We often use the Kirchhoff–Helmholtz integral equation to explain how we predict what we do not measure based on what we do measure. It is noteworthy, however, that the same result can be obtained by using the characteristic solutions of the Helmholtz equation. The following sections address how these can be obtained. Planar, cylindrical, and spherical acoustic holography are derived using characteristic equations in terms of a corresponding coordinate system. The equations for holography are also expressed in a discrete form.

26.A.1 Planar Acoustic Holography

If we see solutions of the Helmholtz equation

$$\nabla^2 P + k^2 P = 0, \quad (26.A1)$$

in terms of Cartesian coordinate, then we can write them as

$$P(x, y, z; f) = X(x)Y(y)Z(z), \quad (26.A2)$$

where $k = \frac{\omega}{c} = \frac{2\pi f}{c}$. We assume then P is separable with respect to X , Y and Z . Equations (26.A1) and

(26.A2) yield the characteristic equation

$$\begin{aligned} \psi(x, y, z; k_x, k_y, k_z) \\ = \begin{pmatrix} e^{ik_x x} \\ e^{-ik_x x} \end{pmatrix} \begin{pmatrix} e^{ik_y y} \\ e^{-ik_y y} \end{pmatrix} \begin{pmatrix} e^{ik_z z} \\ e^{-ik_z z} \end{pmatrix}, \end{aligned} \quad (26.A3)$$

where

$$k^2 = k_x^2 + k_y^2 + k_z^2. \quad (26.A4)$$

Now we can write

$$P(x, y, z; f) = \int \hat{P}(\mathbf{k}) \psi(x, y, z; k_x, k_y, k_z) d\mathbf{k}, \quad (26.A5)$$

where

$$\mathbf{k} = (k_x, k_y, k_z). \quad (26.A6)$$

Let us assume that the sound sources are all located at $z < z_s$ and we measure at $z = z_h > z_s$. Then we can write (26.A5) as

$$\begin{aligned} P(x, y, z; f) \\ = \int_{-\infty}^{\infty} \int_{-\infty}^{\infty} \hat{P}(k_x, k_y) e^{i(k_x x + k_y y + k_z z)} dk_x dk_y. \end{aligned} \quad (26.A7)$$

It is noteworthy that we selected only $+ik_z z$. This is because of the assumptions we made ($z < z_s$ and $z = z_h > z_s$). The k_x and k_y can be either positive or negative. Therefore it is not necessary to include $-ik_x x$ or $-ik_y y$ in (26.A3).

In (26.7),

$$k_z = \begin{cases} \sqrt{k^2 - k_x^2 - k_y^2}, & \text{when } k^2 > k_x^2 + k_y^2 \\ i\sqrt{k_x^2 + k_y^2 - k^2}, & \text{when } k^2 < k_x^2 + k_y^2. \end{cases} \quad (26.A8)$$

Figure 26.6 illustrates what these two different k_z values essentially mean. We measure $P(x, y, z = z_h; f)$, therefore we have data of the sound pressure data on $z = z_h$. A Fourier transform of (26.A7) leads to

$$\begin{aligned} \hat{P}(k_x, k_y) \\ = \int_{-\infty}^{\infty} \int_{-\infty}^{\infty} P(x, y, z; f) e^{-i(k_x x + k_y y + k_z z)} dx dy. \end{aligned} \quad (26.A9)$$

Using (26.A9) and (26.A7), we can always estimate the sound pressure on z , which is away from the source.

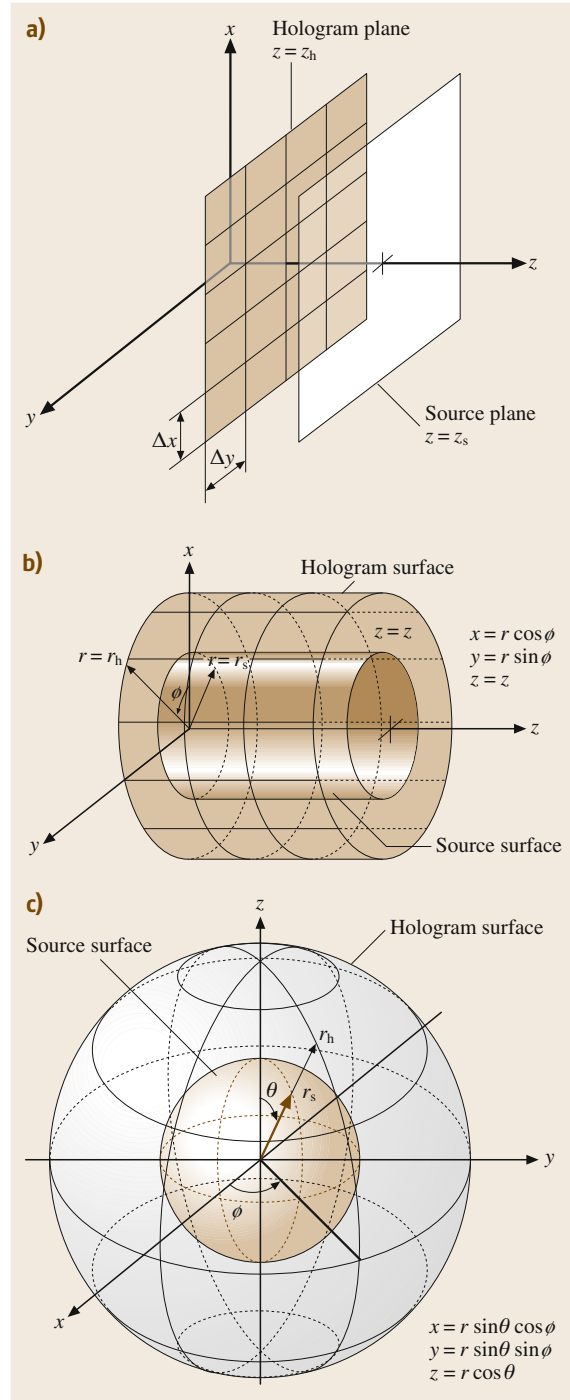


Fig. 26.30a-c Coordinates system for acoustic holography: (a) planar acoustic holography (b) cylindrical acoustic holography (c) spherical acoustic holography

It is noteworthy that (26.A9) has to be preformed in the discrete domain. In other words, we have to use a finite rectangular aperture, which is spatially sampled (26.8 and 26.30a). If the number of measurement points along the x - and y -directions are M and N , respectively, and the corresponding sampling distances are Δx and Δy , then (26.A9) can be rewritten as

$$\hat{P}(k_x, k_y) = \frac{1}{(2\pi)^2} e^{-ik_z z_h} \Delta x \Delta y \sum_{m=0}^{M-1} \sum_{n=0}^{N-1} P(x_m, y_n, z_h) e^{-ik_x x_m} e^{-ik_y y_n} . \quad (26.A10)$$

where

$$x_m = \left(m + \frac{1-M}{2} \right) \Delta x , \quad (26.A11)$$

$$y_n = \left(n + \frac{1-N}{2} \right) \Delta y .$$

M and N are the number of data points in the x - and y -directions, respectively.

26.A.2 Cylindrical Acoustic Holography

A solution can also found in cylindrical coordinate, that is

$$P(r, \phi, z) = R(r)\Phi(\phi)Z(z) . \quad (26.A12)$$

Figure 26.1 shows the coordinate systems. Then, its characteristic solutions are

$$\psi(r, \phi, z; k_r, k_z) = \begin{pmatrix} H_m^{(1)}(k_r r) \\ H_m^{(2)}(k_r r) \end{pmatrix} \begin{bmatrix} e^{im\phi} \\ e^{-im\phi} \end{bmatrix} \begin{bmatrix} e^{ik_z z} \\ e^{-ik_z z} \end{bmatrix} , \quad (26.A13)$$

where

$$k^2 = k_r^2 + k_z^2 . \quad (26.A14)$$

It is noteworthy that m is a nonnegative integer. $H_m^{(1)}$ and $H_m^{(2)}$ are first and second cylindrical Hankel functions, respectively. $e^{im\phi}$ and $e^{-im\phi}$ express the mode shapes in the ϕ -direction.

Using the characteristic function (26.A6), we can write a solution of the Helmholtz equation with respect to cylindrical coordinate as

$$P(r, \phi, z; f) = \int \hat{P}_m(\mathbf{k}) \psi_m(r, \phi, z; k_r, k_z) d\mathbf{k} , \quad (26.A15)$$

where

$$\mathbf{k} = (k_r, k_z) . \quad (26.A16)$$

Assuming that the sound sources are all located at $r < r_s$ and that the hologram surface is situated on the surface $r = r_h$, and that $r_h > r_s$, then no waves propagate into the negative r -direction, in other words, toward the sources. Then (26.A15) can be rewritten as

$$P(r, \phi, z; f) = \sum_{m=-\infty}^{\infty} \int_{-\infty}^{\infty} \hat{P}_m(k_z) e^{im\phi} e^{ik_z z} H_m^{(1)}(k_r r) dk_z , \quad (26.A17)$$

and k_r has to be

$$k_r = \begin{cases} \sqrt{k^2 - k_z^2} , & \text{when } k^2 > k_z^2 \\ i\sqrt{k_z^2 - k^2} , & \text{when } k^2 < k_z^2 . \end{cases} \quad (26.A18)$$

We measure the acoustic pressure at $r = r_h$, therefore $P(r_h, \phi, z)$ is available. $\hat{P}_m(k_z)$ can then be readily obtained.

That is

$$\hat{P}_m(k_z) = \frac{1}{(2\pi)^2} \int_0^{2\pi} \int_{-\infty}^{\infty} P(r_h, \phi, z) e^{-m\phi} e^{-ik_z z} \times \left\{ H_m^{(1)}(k_r r_h) \right\}^{-1} dz d\phi . \quad (26.A19)$$

Inserting (26.A19) into (26.A17) provides us with the acoustic pressure at the unmeasured surface at r .

Discretization of (26.A19) leads to a formula that can be used in practical calculations

$$\hat{P}_m(k_z) = \frac{1}{(2\pi)^2 H_m^{(1)}(k_r r_h)} \frac{2\pi}{L} \Delta z \times \sum_{l=0}^{L-1} \sum_{n=0}^{N-1} P(r_h, \phi_l, z_n) e^{-im\phi_l} e^{-ik_z z_n} , \quad (26.A20)$$

where

$$\phi_l = \frac{(2l+1)\pi}{L} , \quad (26.A21)$$

$$z_n = \left(n + \frac{1-N}{2} \right) \Delta z .$$

L and N are the number of data points in the ϕ - and z -directions, respectively.

26.A.3 Spherical Acoustic Holography

The Helmholtz equation can also be expressed in spherical coordinate (Fig. 26.30c). Assuming again that the separation of variable also holds in this case, we can write

$$P(r, \theta, \phi) = R(r)\Theta(\theta)\Phi(\phi). \quad (26.A22)$$

Substituting this into (26.A1) gives the characteristic equation

$$\psi_{mn}(r, \theta, \phi; k) = \begin{pmatrix} h_m^{(1)}(kr) \\ h_m^{(2)}(kr) \end{pmatrix} \begin{pmatrix} P_m^n \cos \theta \\ Q_m^n \cos \theta \end{pmatrix} \begin{pmatrix} e^{in\phi} \\ e^{-in\phi} \end{pmatrix}. \quad (26.A23)$$

m is a nonnegative integer and n can be any integer between 0 and m . $h_m^{(1)}$ and $h_m^{(2)}$ are first and second spherical Hankel functions. It is also noteworthy that P_m^n and Q_m^n are first and second Legendre polynomials.

Then we can write the solution of the Helmholtz equation as

$$P(r, \theta, \phi) = \sum_{m=0}^{\infty} \sum_{n=-m}^m \hat{P}_{mn} \psi_{mn}(r, \theta, \phi; k). \quad (26.A24)$$

Suppose that we have sound sources at $r < r_s$ and the hologram is on the surface $r = r_h > r_s$; then (26.A24) can be simplified to

$$P(r, \theta, \phi) = \sum_{m=0}^{\infty} \sum_{n=-m}^m \hat{P}_{mn} Y_{mn}(\theta, \phi) h_m^{(1)}(kr), \quad (26.A25)$$

where

$$Y_{mn}(\theta, \phi) = P_m^{|n|}(\cos \theta) e^{in\phi}. \quad (26.A26)$$

This is a spherical harmonic function. It is noteworthy that we only have first spherical harmonic functions because all waves propagate away from the sources. The second Legendre function was discarded because it would have finite acoustic pressure at $\theta = 0$ or π .

Similarly, as previously stated, the sound pressure data on the hologram is available, therefore we can obtain P_{mn} in (26.A25) by

$$\hat{P}_{mn} = \frac{2m+1}{4\pi h_m^{(1)}(kr_h)} \frac{(m-|n|)!}{(m+|n|)!} \times \int_0^\pi \int_0^{2\pi} P(r_h, \theta, \phi) Y_{mn}^*(\theta, \phi) \sin \theta d\phi d\theta, \quad (26.A27)$$

where we have used the orthogonality property of Y_{mn} . The $*$ represents the complex conjugate. Using (26.A27) and (26.A25), we can estimate the acoustic pressure anywhere away from the sources.

The discrete form of (26.A27) can be written as

$$\hat{P}_{mn} = A_{mn} \frac{2\pi^2}{LQ} \sum_{l=0}^{L-1} \sum_{q=0}^{Q-1} P(r_h, \theta_l, \phi_q) \times P_m^{|n|}(\cos \theta_l) (\sin \theta_l) e^{-in\phi_q}, \quad (26.A28)$$

where

$$\theta_l = \frac{(2l+1)\pi}{2L}, \quad \phi_q = \frac{(2q+1)\pi}{Q}. \quad (26.A29)$$

where L is the number of data points in θ and Q is what is in ϕ -direction.

References

- | | |
|--|--|
| <p>26.1 M. Kac: Can one hear the shape of the drum?, Am. Math. Mon. 73, 1–23 (1966)</p> <p>26.2 G.T. Herman, H.K. Tuy, K.J. Langenberg: <i>Basic Methods of Tomography and Inverse Problems</i> (Malvern, Philadelphia 1987)</p> <p>26.3 H.D. Bui: <i>Inverse Problems in the Mechanics of Materials: An Introduction</i> (CRC, Boca Raton 1994)</p> <p>26.4 K. Kurpisz, A.J. Nowak: <i>Inverse Thermal Problems</i> (Computational Mechanics Publ., Southampton 1995)</p> <p>26.5 A. Kirsch: <i>An Introduction to the Mathematical Theory of Inverse Problems</i> (Springer, Berlin, Heidelberg 1996)</p> | <p>26.6 M. Bertero, P. Boccacci: <i>Introduction to Inverse Problems in Imaging</i> (IOP, Bristol 1998)</p> <p>26.7 V. Isakov: <i>Inverse Problems for Partial Differential Equations</i> (Springer, New York 1998)</p> <p>26.8 D.N. Ghosh Roy, L.S. Couchman: <i>Inverse Problems and Inverse Scattering of Plane Waves</i> (Academic, New York 2002)</p> <p>26.9 J. Hardamard: <i>Lectures on Cauchy's Problem in Linear Partial Differential Equations</i> (Yale Univ. Press, New Haven 1923)</p> <p>26.10 L. Landweber: An iteration formula for Fredholm integral equations of the first kind, Am. J. Math. 73, 615–624 (1951)</p> |
|--|--|

- 26.11 A.M. Cormack: Representation of a function by its line integrals, with some radiological applications, *J. App. Phys.* **34**, 2722–2727 (1963)
- 26.12 A.M. Cormack: Representation of a function by its line integrals, with some radiological applications II, *J. App. Phys.* **35**, 2908–2913 (1964)
- 26.13 A.N. Tikhonov, V.Y. Arsenin: *Solutions of Ill-Posed Problems* (Winston, Washington 1977)
- 26.14 S.R. Deans: *The Radon Transform and Some of its Applications* (Wiley, New York 1983)
- 26.15 A.K. Louis: Mathematical problems of computerized tomography, *Proc. IEEE*, Vol. 71 (1983) pp. 379–389
- 26.16 M.H. Protter: Can one hear the shape of a drum? Revisited, *SIAM Rev.* **29**, 185–197 (1987)
- 26.17 K. Chadan, P.C. Sabatier: *Inverse Problems in Quantum Scattering Theory*, 2nd edn. (Springer, New York 1989)
- 26.18 A.K. Louis: Medical imaging: state of the art and future development, *Inv. Probl.* **8**, 709–738 (1992)
- 26.19 D. Colton, R. Kress: *Inverse Acoustic and Electromagnetic Scattering Theory*, 2nd edn. (Springer, New York 1998)
- 26.20 D. Gabor: A new microscopic principle, *Nature* **161**, 777 (1948)
- 26.21 B.P. Hilderbrand, B.B. Brenden: *An Introduction to Acoustical Holography* (Plenum, New York 1972)
- 26.22 E.N. Leith, J. Upatnieks: Reconstructed wavefronts and communication theory, *J. Opt. Soc. Am.* **52**, 1123–1130 (1962)
- 26.23 W.E. Kock: Hologram television, *Proc. IEEE*, Vol. 54 (1966) p. 331
- 26.24 G. Tricoles, E.L. Rope: Reconstructions of visible images from reduced-scale replicas of microwave holograms, *J. Opt. Soc. Am.* **57**, 97–99 (1967)
- 26.25 G.C. Sherman: Reconstructed wave forms with large diffraction angles, *J. Opt. Soc. Am.* **57**, 1160–1161 (1967)
- 26.26 J.W. Goodman, R.W. Lawrence: Digital image formation from electronically detected holograms, *Appl. Phys. Lett.* **11**, 77–79 (1967)
- 26.27 Y. Aoki: Microwave holograms and optical reconstruction, *Appl. Opt.* **6**, 1943–1946 (1967)
- 26.28 R.P. Porter: Diffraction-limited, scalar image formation with holograms of arbitrary shape, *J. Opt. Soc. Am.* **60**, 1051–1059 (1970)
- 26.29 E. Wolf: Determination of the amplitude and the phase of scattered fields by holography, *J. Opt. Soc. Am.* **60**, 18–20 (1970)
- 26.30 W.H. Carter: Computational reconstruction of scattering objects from holograms, *J. Opt. Soc. Am.* **60**, 306–314 (1970)
- 26.31 E.G. Williams, J.D. Maynard, E. Skudrzyk: Sound source reconstruction using a microphone array, *J. Acoust. Soc. Am.* **68**, 340–344 (1980)
- 26.32 E.G. Williams, J.D. Maynard: Holographic imaging without the wavelength resolution limit, *Phys. Rev. Lett.* **45**, 554–557 (1980)
- 26.33 E.A. Ash, G. Nichols: Super-resolution aperture scanning microscope, *Nature* **237**, 510–512 (1972)
- 26.34 S.U. Pillai: *Array Signal Processing* (Springer, New York 1989)
- 26.35 D.H. Johnson, D.E. Dudgeon: *Array Signal Processing Concepts and Techniques* (Prentice-Hall, Upper Saddle River 1993)
- 26.36 M. Kaveh, A.J. Barabell: The statistical performance of the MUSIC and the minimum-Norm algorithms in resolving plane waves in noise, *IEEE Trans. Acoust. Speech Signal Process.* **34**, 331–341 (1986)
- 26.37 M. Lasky: Review of undersea acoustics to 1950, *J. Acoust. Soc. Am.* **61**, 283–297 (1977)
- 26.38 B. Barskow, W.F. King, E. Pfizenmaier: Wheel/rail noise generated by a high-speed train investigated with a line array of microphones, *J. Sound Vib.* **118**, 99–122 (1987)
- 26.39 J. Hald, J.J. Christensen: A class of optimal broadband phased array geometries designed for easy construction, *Proc. Inter-Noise 2002* (Int. Inst. Noise Control Eng., West Lafayette 2002)
- 26.40 Y. Takano: Development of visualization system for high-speed noise sources with a microphone array and a visual sensor, *Proc. Inter-Noise 2003* (Int. Inst. Noise Control Eng., West Lafayette 2003)
- 26.41 G. Elias: Source localization with a two-dimensional focused array: Optimal signal processing for a cross-shaped array, *Proc. Inter-Noise 95* (Int. Inst. Noise Control Eng., West Lafayette 1995) pp. 1175–1178
- 26.42 A. Nordborg, A. Martens, J. Wedemann, L. Wellenbrink: Wheel/rail noise separation with microphone array measurements, *Proc. Inter-Noise 2001* (Int. Inst. Noise Control Eng., West Lafayette 2001) pp. 2083–2088
- 26.43 A. Nordborg, J. Wedemann, L. Wellenbrink: Optimum array microphone configuration, *Proc. Inter-Noise 2000* (Int. Inst. Noise Control Eng., West Lafayette 2000)
- 26.44 P.R. Stepanishen, K.C. Benjamin: Forward and backward prediction of acoustic fields using FFT methods, *J. Acoust. Soc. Am.* **71**, 803–812 (1982)
- 26.45 E.G. Williams, J.D. Maynard: Numerical evaluation of the Rayleigh integral for planar radiators using the FFT, *J. Acoust. Soc. Am.* **72**, 2020–2030 (1982)
- 26.46 J.D. Maynard, E.G. Williams, Y. Lee: Nearfield acoustic holography (NAH): I. Theory of generalized holography and the development of NAH, *J. Acoust. Soc. Am.* **78**, 1395–1413 (1985)
- 26.47 W.A. Veronesi, J.D. Maynard: Nearfield acoustic holography (NAH) II. Holographic reconstruction algorithms and computer implementation, *J. Acoust. Soc. Am.* **81**, 1307–1322 (1987)

- 26.48 S.I. Hayek, T.W. Luce: Aperture effects in planar nearfield acoustical imaging, *ASME J. Vib. Acoust. Stress Reliab. Des.* **110**, 91–96 (1988)
- 26.49 A. Sarkissian, C.F. Gaumont, E.G. Williams, B.H. Houston: Reconstruction of the acoustic field over a limited surface area on a vibrating cylinder, *J. Acoust. Soc. Am.* **93**, 48–54 (1993)
- 26.50 J. Hald: Reduction of spatial windowing effects in acoustical holography, *Proc. Inter-Noise 94 (Int. Inst. Noise Control Eng., West Lafayette 1994)* pp.1887–1890
- 26.51 H.-S. Kwon, Y.-H. Kim: Minimization of bias error due to windows in planar acoustic holography using a minimum error window, *J. Acoust. Soc. Am.* **98**, 2104–2111 (1995)
- 26.52 K. Saijou, S. Yoshikawa: Reduction methods of the reconstruction error for large-scale implementation of near-field acoustical holography, *J. Acoust. Soc. Am.* **110**, 2007–2023 (2001)
- 26.53 K.-U. Nam, Y.-H. Kim: Errors due to sensor and position mismatch in planar acoustic holography, *J. Acoust. Soc. Am.* **106**, 1655–1665 (1999)
- 26.54 G. Weinreich, E.B. Arnold: Method for measuring acoustic radiation fields, *J. Acoust. Soc. Am.* **68**, 404–411 (1980)
- 26.55 E.G. Williams, H.D. Dardy, R.G. Fink: Nearfield acoustical holography using an underwater, automated scanner, *J. Acoust. Soc. Am.* **78**, 789–798 (1985)
- 26.56 D. Blacodon, S.M. Candel, G. Elias: Radial extrapolation of wave fields from synthetic measurements of the nearfield, *J. Acoust. Soc. Am.* **82**, 1060–1072 (1987)
- 26.57 J. Hald: *STSF – a unique technique for scan-based near-field acoustic holography without restrictions on coherence*, *Bruel Kjaer Tech. Rev. 1 (Bruel Kjaer, Noerum 1989)*
- 26.58 K.B. Ginn, J. Hald: *STSF – practical instrumentation and applications*, *Bruel Kjaer Tech. Rev. 2 (Bruel Kjaer, Noerum 1989)*
- 26.59 S.H. Yoon, P.A. Nelson: A method for the efficient construction of acoustic pressure cross-spectral matrices, *J. Sound Vib.* **233**, 897–920 (2000)
- 26.60 H.-S. Kwon, Y.-J. Kim, J.S. Bolton: Compensation for source nonstationarity in multireference, scan-based near-field acoustical holography, *J. Acoust. Soc. Am.* **113**, 360–368 (2003)
- 26.61 K.-U. Nam, Y.-H. Kim: Low coherence acoustic holography, *Proc. Inter-Noise 2003 (Int. Inst. Noise Control Eng., West Lafayette 2003)*
- 26.62 H.-S. Kwon, Y.-H. Kim: Moving frame technique for planar acoustic holography, *J. Acoust. Soc. Am.* **103**, 1734–1741 (1998)
- 26.63 S.-H. Park, Y.-H. Kim: An improved moving frame acoustic holography for coherent band-limited noise, *J. Acoust. Soc. Am.* **104**, 3179–3189 (1998)
- 26.64 S.-H. Park, Y.-H. Kim: Effects of the speed of moving noise sources on the sound visualization by means of moving frame acoustic holography, *J. Acoust. Soc. Am.* **108**, 2719–2728 (2000)
- 26.65 S.-H. Park, Y.-H. Kim: Visualization of pass-by noise by means of moving frame acoustic holography, *J. Acoust. Soc. Am.* **110**, 2326–2339 (2001)
- 26.66 S.M. Candel, C. Chassignon: Radial extrapolation of wave fields by spectral methods, *J. Acoust. Soc. Am.* **76**, 1823–1828 (1984)
- 26.67 E.G. Williams, H.D. Dardy, K.B. Washburn: Generalized nearfield acoustical holography for cylindrical geometry: Theory and experiment, *J. Acoust. Soc. Am.* **81**, 389–407 (1987)
- 26.68 B.K. Gardner, R.J. Bernhard: A noise source identification technique using an inverse Helmholtz integral equation method, *ASME J. Vib. Acoust. Stress Reliab. Des.* **110**, 84–90 (1988)
- 26.69 E.G. Williams, B.H. Houston, J.A. Bucaro: Broad-band nearfield acoustical holography for vibrating cylinders, *J. Acoust. Soc. Am.* **86**, 674–679 (1989)
- 26.70 G.H. Koopmann, L. Song, J.B. Fahnlne: A method for computing acoustic fields based on the principle of wave superposition, *J. Acoust. Soc. Am.* **86**, 2433–2438 (1989)
- 26.71 A. Sarkissian: Near-field acoustic holography for an axisymmetric geometry: A new formulation, *J. Acoust. Soc. Am.* **88**, 961–966 (1990)
- 26.72 M. Tamura: Spatial Fourier transform method of measuring reflection coefficients at oblique incidence. I: Theory and numerical examples, *J. Acoust. Soc. Am.* **88**, 2259–2264 (1990)
- 26.73 L. Song, G.H. Koopmann, J.B. Fahnlne: Numerical errors associated with the method of superposition for computing acoustic fields, *J. Acoust. Soc. Am.* **89**, 2625–2633 (1991)
- 26.74 M. Villot, G. Chaveriat, J. Ronald: Phonoscopy: An acoustical holography technique for plane structures radiating in enclosed spaces, *J. Acoust. Soc. Am.* **91**, 187–195 (1992)
- 26.75 D.L. Hallman, J.S. Bolton: Multi-reference nearfield acoustical holography in reflective environments, *Proc. Inter-Noise 93 (Int. Inst. Noise Control Eng., West Lafayette 1993)* pp.1307–1310
- 26.76 M.-T. Cheng, J.A. Mann III, A. Pate: Wave-number domain separation of the incident and scattered sound field in Cartesian and cylindrical coordinates, *J. Acoust. Soc. Am.* **97**, 2293–2303 (1995)
- 26.77 M. Tamura, J.F. Allard, D. Lafarge: Spatial Fourier-transform method for measuring reflection coefficients at oblique incidence. II. Experimental results, *J. Acoust. Soc. Am.* **97**, 2255–2262 (1995)
- 26.78 Z. Wang, S.F. Wu: Helmholtz equation – least-squares method for reconstructing the acoustic pressure field, *J. Acoust. Soc. Am.* **102**, 2020–2032 (1997)
- 26.79 S.F. Wu, J. Yu: Reconstructing interior acoustic pressure fields via Helmholtz equation least-

- squares method, *J. Acoust. Soc. Am.* **104**, 2054–2060 (1998)
- 26.80 S.-C. Kang, J.-G. Ih: The use of partially measured source data in near-field acoustical holography based on the BEM, *J. Acoust. Soc. Am.* **107**, 2472–2479 (2000)
- 26.81 S.F. Wu: On reconstruction of acoustic pressure fields using the Helmholtz equation least squares method, *J. Acoust. Soc. Am.* **107**, 2511–2522 (2000)
- 26.82 N. Rayess, S.F. Wu: Experimental validation of the HELS method for reconstructing acoustic radiation from a complex vibrating structure, *J. Acoust. Soc. Am.* **107**, 2955–2964 (2000)
- 26.83 Z. Zhang, N. Vlahopoulos, S.T. Raveendra, T. Allen, K.Y. Zhang: A computational acoustic field reconstruction process based on an indirect boundary element formulation, *J. Acoust. Soc. Am.* **108**, 2167–2178 (2000)
- 26.84 S.-C. Kang, J.-G. Ih: On the accuracy of nearfield pressure predicted by the acoustic boundary element method, *J. Sound Vib.* **233**, 353–358 (2000)
- 26.85 S.-C. Kang, J.-G. Ih: Use of nonsingular boundary integral formulation for reducing errors due to near-field measurements in the boundary element method based near-field acoustic holography, *J. Acoust. Soc. Am.* **109**, 1320–1328 (2001)
- 26.86 S.F. Wu, N. Rayess, X. Zhao: Visualization of acoustic radiation from a vibrating bowling ball, *J. Acoust. Soc. Am.* **109**, 2771–2779 (2001)
- 26.87 J.D. Maynard: A new technique combining eigenfunction expansions and boundary elements to solve acoustic radiation problems, *Proc. Inter-Noise 2003 (Int. Inst. Noise Control Eng., West Lafayette 2003)*
- 26.88 E.G. Williams: *Fourier Acoustics: Sound Radiation and Near Field Acoustical Holography* (Academic, London 1999)
- 26.89 F.L. Thurstone: Ultrasound holography and visual reconstruction, *Proc. Symp. Biomed. Eng., Vol.1 (1966)* pp.12–15
- 26.90 A.L. Boyer, J.A. Jordan Jr., D.L. van Rooy, P.M. Hirsch, L.B. Lesem: Computer reconstruction of images from ultrasonic holograms, *Proc. Second Int. Symp. Acoust. Hologr. (Plenum, New York 1969)*
- 26.91 A.F. Metilerell, H.M.A. El-Sum, J.J. Dreher, L. Larmore: Introduction to acoustical holography, *J. Acoust. Soc. Am.* **42**, 733–742 (1967)
- 26.92 L.A. Cram, K.O. Rossiter: Long-wavelength holography and visual reproduction methods, *Proc. Second Int. Symp. Acoust. Hologr. (Plenum, New York 1969)*
- 26.93 T.S. Graham: A new method for studying acoustic radiation using long-wavelength acoustical holography, *Proc. Second Int. Symp. Acoust. Hologr. (Plenum, New York 1969)*
- 26.94 E.E. Watson: Detection of acoustic sources using long-wavelength acoustical holography, *J. Acoust. Soc. Am.* **54**, 685–691 (1973)
- 26.95 H. Fleischer, V. Axelrad: Restoring an acoustic source from pressure data using Wiener filtering, *Acustica* **60**, 172–175 (1986)
- 26.96 E.G. Williams: Supersonic acoustic intensity, *J. Acoust. Soc. Am.* **97**, 121–127 (1995)
- 26.97 M.R. Bai: Acoustical source characterization by using recursive Wiener filtering, *J. Acoust. Soc. Am.* **97**, 2657–2663 (1995)
- 26.98 J.C. Lee: Spherical acoustical holography of low-frequency noise sources, *Appl. Acoust.* **48**, 85–95 (1996)
- 26.99 G.P. Carroll: The effect of sensor placement errors on cylindrical near-field acoustic holography, *J. Acoust. Soc. Am.* **105**, 2269–2276 (1999)
- 26.100 W.A. Veronesi, J.D. Maynard: Digital holographic reconstruction of sources with arbitrarily shaped surfaces, *J. Acoust. Soc. Am.* **85**, 588–598 (1989)
- 26.101 G.V. Borgiotti, A. Sarkissan, E.G. Williams, L. Schuetz: Conformal generalized near-field acoustic holography for axisymmetric geometries, *J. Acoust. Soc. Am.* **88**, 199–209 (1990)
- 26.102 D.M. Photiadis: The relationship of singular value decomposition to wave-vector filtering in sound radiation problems, *J. Acoust. Soc. Am.* **88**, 1152–1159 (1990)
- 26.103 G.-T. Kim, B.-H. Lee: 3-D sound source reconstruction and field prediction using the Helmholtz integral equation, *J. Sound Vib.* **136**, 245–261 (1990)
- 26.104 A. Sarkissan: Acoustic radiation from finite structures, *J. Acoust. Soc. Am.* **90**, 574–578 (1991)
- 26.105 J.B. Fahnlne, G.H. Koopmann: A numerical solution for the general radiation problem based on the combined methods of superposition and singular value decomposition, *J. Acoust. Soc. Am.* **90**, 2808–2819 (1991)
- 26.106 M.R. Bai: Application of BEM (boundary element method)-based acoustic holography to radiation analysis of sound sources with arbitrarily shaped geometries, *J. Acoust. Soc. Am.* **92**, 533–549 (1992)
- 26.107 G.V. Borgiotti, E.M. Rosen: The determination of the far field of an acoustic radiator from sparse measurement samples in the near field, *J. Acoust. Soc. Am.* **92**, 807–818 (1992)
- 26.108 B.-K. Kim, J.-G. Ih: On the reconstruction of the vibro-acoustic field over the surface enclosing an interior space using the boundary element method, *J. Acoust. Soc. Am.* **100**, 3003–3016 (1996)
- 26.109 B.-K. Kim, J.-G. Ih: Design of an optimal wave-vector filter for enhancing the resolution of reconstructed source field by near-field acoustical holography (NAH), *J. Acoust. Soc. Am.* **107**, 3289–3297 (2000)
- 26.110 P.A. Nelson, S.H. Yoon: Estimation of acoustic source strength by inverse methods: Part I, condi-

- tioning of the inverse problem, *J. Sound Vib.* **233**, 643–668 (2000)
- 26.111 S.H. Yoon, P.A. Nelson: Estimation of acoustic source strength by inverse methods: Part II, experimental investigation of methods for choosing regularization parameters, *J. Sound Vib.* **233**, 669–705 (2000)
- 26.112 E.G. Williams: Regularization methods for near-field acoustical holography, *J. Acoust. Soc. Am.* **110**, 1976–1988 (2001)
- 26.113 S.F. Wu, X. Zhao: Combined Helmholtz equation – least squares method for reconstructing acoustic radiation from arbitrarily shaped objects, *J. Acoust. Soc. Am.* **112**, 179–188 (2002)
- 26.114 A. Schuhmacher, J. Hald, K.B. Rasmussen, P.C. Hansen: Sound source reconstruction using inverse boundary element calculations, *J. Acoust. Soc. Am.* **113**, 114–127 (2003)
- 26.115 Y. Kim, P.A. Nelson: Spatial resolution limits for the reconstruction of acoustic source strength by inverse methods, *J. Sound Vib.* **265**, 583–608 (2003)
- 26.116 Y.-K. Kim, Y.-H. Kim: Holographic reconstruction of active sources and surface admittance in an enclosure, *J. Acoust. Soc. Am.* **105**, 2377–2383 (1999)
- 26.117 P.M. Morse, H. Feshbach: *Methods of Theoretical Physics, Part I* (McGraw–Hill, New York 1992)
- 26.118 L.L. Beranek, I.L. Ver: *Noise and Vibration Control Engineering* (Wiley, New York 1992)
- 26.119 J.S. Bendat, A.G. Piersol: *Random Data: Analysis and Measurement Procedures*, 2nd edn. (Wiley, New York 1986)
- 26.120 D. Hallman, J.S. Bolton: Multi-reference nearfield acoustical holography, *Proc. Inter-Noise 92* (Int. Inst. Noise Control Eng., West Lafayette 1992) pp. 1165–1170
- 26.121 R.J. Ruhala, C.B. Burroughs: Separation of leading edge, trailing edge, and sidewall noise sources from rolling tires, *Proc. Noise-Con 98* (Noise Control Foundation, Poughkeepsie 1998) pp. 109–114
- 26.122 H.-S. Kwon, J.S. Bolton: Partial field decomposition in nearfield acoustical holography by the use of singular value decomposition and partial coherence procedures, *Proc. Noise-Con 98* (Noise Control Foundation, Poughkeepsie 1998) pp. 649–654
- 26.123 M.A. Tomlinson: Partial source discrimination in near field acoustic holography, *Appl. Acoust.* **57**, 243–261 (1999)
- 26.124 K.-U. Nam, Y.-H. Kim: Visualization of multiple incoherent sources by the backward prediction of near-field acoustic holography, *J. Acoust. Soc. Am.* **109**, 1808–1816 (2001)
- 26.125 K.-U. Nam, Y.-H. Kim, Y.-C. Choi, D.-W. Kim, O.-J. Kwon, K.-T. Kang, S.-G. Jung: Visualization of speaker, vortex shedding, engine, and wind noise of a car by partial field decomposition, *Proc. Inter-Noise 2002* (Int. Inst. Noise Control Eng., West Lafayette 2002)